AD_____

Award Number: W81XWH-06-1-0271

TITLE: Development of a Smart Diagnostics Platform for Early-Stage Screening of Breast Cancer

PRINCIPAL INVESTIGATOR: Joerg Lahann

CONTRACTING ORGANIZATION: University of Michigan
Ann Arbor, MI 48109

REPORT DATE: April 2007

TYPE OF REPORT: Annual

PREPARED FOR: U.S. Army Medical Research and Materiel Command
Fort Detrick, Maryland 21702-5012

DISTRIBUTION STATEMENT: Approved for Public Release;
Distribution Unlimited

REPORT DOCUMENTATION PAGE

Form Approved
OMB No. 0704-0188

1. REPORT DATE	2. REPORT TYPE	3. DATES COVERED
01-04-2007	Annual	1 Apr 2006 – 31Mar 2007

4. TITLE AND SUBTITLE

Development of a Smart Diagnostics Platform for Early-Stage Screening of Breast Cancer

5a. CONTRACT NUMBER

5b. GRANT NUMBER
W81XWH-06-1-0271

5c. PROGRAM ELEMENT NUMBER

6. AUTHOR(S)

Joerg Lahann

Email: lahann@umich.edu

5d. PROJECT NUMBER

5e. TASK NUMBER

5f. WORK UNIT NUMBER

7. PERFORMING ORGANIZATION NAME(S) AND ADDRESS(ES)

University of Michigan
Ann Arbor, MI 48109

8. PERFORMING ORGANIZATION REPORT NUMBER

9. SPONSORING / MONITORING AGENCY NAME(S) AND ADDRESS(ES)
U.S. Army Medical Research and Materiel Command
Fort Detrick, Maryland 21702-5012

10. SPONSOR/MONITOR'S ACRONYM(S)

11. SPONSOR/MONITOR'S REPORT NUMBER(S)

12. DISTRIBUTION / AVAILABILITY STATEMENT
Approved for Public Release; Distribution Unlimited

13. SUPPLEMENTARY NOTES
Original contains colored plates: ALL DTIC reproductions will be in black and white.

14. ABSTRACT

The proposed research aims to develop innovative technology that could ultimately lead to new breast cancer screening tests — ones, which will not require expensive equipment for read-out, but rather will be compatible with miniaturized systems integrated in cheap handheld devices. Towards this goal, we have designed and realized in practice a surface that can act as detection unit. This opens the door for further work that will be geared towards testing of biomarkers.

15. SUBJECT TERMS
Breast Cancer

16. SECURITY CLASSIFICATION OF:			17. LIMITATION OF ABSTRACT	18. NUMBER OF PAGES	19a. NAME OF RESPONSIBLE PERSON
a. REPORT	b. ABSTRACT	c. THIS PAGE			USAMRMC
U	U	U	UU	28	19b. TELEPHONE NUMBER *(include area code)*

Table of Contents

Page

A. INTRODUCTION.

In the last thirty years, the fight against breast cancer has made impressive strides in diagnosis and treatment. Because of the essential importance that early detection has for successful therapy, the American Cancer Society currently recommends that women over the age of 20 should have a clinical breast exam every three years and that women over the age of 40 should have annual screening mammograms and clinical breast exams. Although current screening methods save thousands of lives each year, they are costly and in some cases ineffective. The proposed research aims to develop innovative technology that could ultimately lead to new breast cancer screening tests which will be compatible with miniaturized systems integrated in cheap handheld devices suitable for widespread screening of large population groups. Ultimately, the technology may allow for screening of cancer-indicative biomarkers in the urine or the breath, thereby establishing non-invasive avenues for screening. The bioindicators that we are targeting are apolar metabolites indicative of early-stage breast cancer. The unique structure of our low-density self-assembled monolayers provides a nano-porous structure that can capture such hydrophobic target molecules, causing measurable changes in surface properties (e.g., changes in the electrical resistance or impedance). Modification of the functional groups may allow customized selectivity to be engineered into the surfaces. If required, the unique switching function of “smart surfaces” can potentially be used to regenerate the sensor surface and confer re-usability to the device. The mono-molecular thickness of the sensor surface also yields the potential for part-per-million sensitivity. The current methods used to analyze bioindicators in urine and breath include high-performance liquid chromatography, gas chromatography, mass spectrometry, and enzyme-linked immunosorbent assay. All of these methods require sophisticated laboratory instrumentation and are not compatible with widespread, in-home screening of large population groups. It’s the ultimate goal of this *Idea Award* proposal to conduct a proof-of-concept study of the first-time design and evaluation of switchable signal transduction units for screening of breast-cancer indicative biomarkers.

B. Body.

Under this *Idea Award* proposal, we intend to develop basic technology for screening of metabolites in a complex environment such as breath or urine. This goal shall be achieved by designing surfaces with nano-scale architecture and porosity ("smart surfaces") that can undergo conformational switching due to the application of external stimuli. Our specific design hypothesis is that the proper molecular design of these "smart surfaces" will lead to surfaces with dynamically controlled binding events of metabolites indicative of early-stage breast cancer (Figure 1). In contrast to conventional screening approaches, a screening platform that relies on "smart surfaces" for signal transduction will have improved ability to be operated in a complicated environment, such as urine or breath, and thus will be amenable to widespread screening of large population groups. Moreover, the proposed "smart surfaces" can be recharged to ensure continuous sampling. This feature may prove to be critical when sensing metabolites, which may undergo less specific binding events than proteins or DNA, currently used in blood tests.

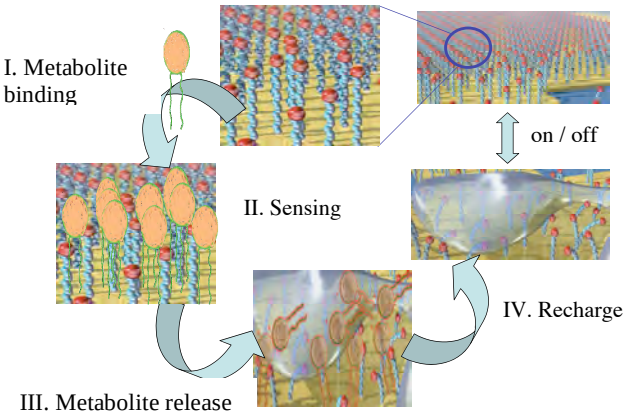

Fig. 1. *Schematic representation of a Smart Diagnostics Platform based on intercalation. The key elements are switchable (smart) surfaces, which enable the modulation of the dynamic sensing range and make the surface rechargeable. Smart surfaces can be switched between nano-porous and collapsed states with the nano-porous state designed to specifically accept apolar bioindicators (but not proteins). After switching and associated monolayer collapse, the indicators are released and subject to secondary screen; the platform is recharged.*

Proposed Approach.

In accordance with the guidelines of the *Idea Award*, this project has been developed as a pilot study to evaluate the feasibility of "smart surfaces" for screening of early-stage breast cancer markers.

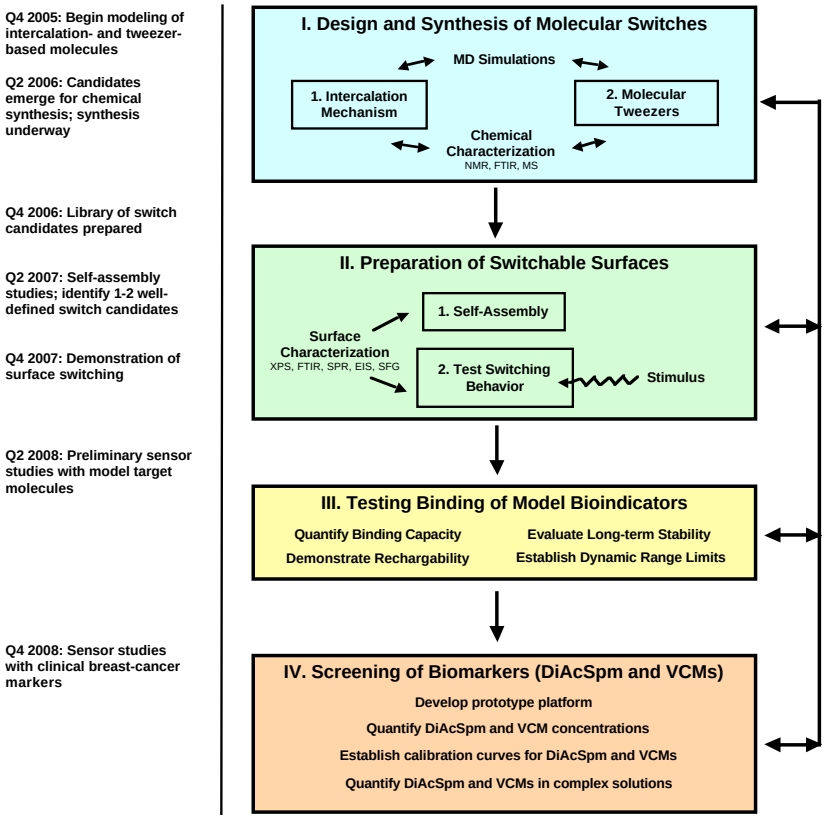

Scheme 1: *Originally proposed outline of the proposed activities towards "smart surfaces" technology.*

While the potential impact of such a technology would be enormous, the proposal is associated with considerable risk. However, we believe that the anticipated progress towards the overarching goal of our program - the development of widely-applicable, non-invasive, and cost-effective diagnostic tools for early-stage metabolic indicators of breast cancer – will far outweigh these risks. One of the major scientific limitations of this project is that it focuses solely on *in vitro* studies. Any meaningful effort in the field requires confirmation by animal studies, and eventually also by clinical studies. However, these efforts are very expensive and must be of a collaborative nature. We will leverage the data obtained in this study to obtain NIH funding for follow-up activities. The following section describes the detailed methods proposed to realize our four objectives.

WORK DONE TOWARDS SPECIFIC AIM #1:

DESIGN AND SYNTHESIS OF MOLECULAR SWITCHES WITH SELECTIVE BINDING PROPERTIES FOR BIOINDICATORS.

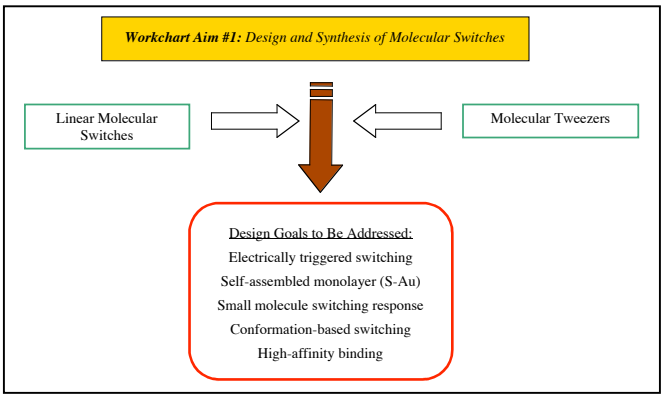

Synthesis of Linear Molecular Switches.

Initially, low-density self-assembled monolayers (LDSAMs) of 16-chlorotrityl-mercaptohexadecanoic acid (CT-MHA) and 16-chlorotrityl-mercaptoundecanoic acid (CT-MUA) were syntheisized with the intend to prepare self-assembled monolayers of linear molecular switches on gold and silver electrodes. Figure 2 outlines the synthetic method for preparing regular SAMs of MHA and MUA as well as the indirect assembly method for preparing LDSAMs as detailed in a recent publication.[1] The indirect method was designed to circumvent the tendency of alkanethiolates to form tightly-packed assemblies resembling two-dimensional crystals.[2,3] The approach involves a multi-step process of conjugating MHA or MUA to bulky, space-filling chlorotrityl (CT) groups to form CT-MHA or CT-MUA esters. The subsequent assembly of CT-MHA or CT-MUA monolayers on gold or silver is followed by cleavage of the bulky CT groups, resulting in LDSAMs of MHA and MUA that are chemically identical to regular SAMs, but differ from the latter in the molecular spacing between the chains.

The synthesis of 16-chlorotrityl-mercaptohexadecanoic acid (CT-MHA) has been reported previously[4] and has now been extended to other variants (MUA). The synthesis of 16-chlorotrityl-mercaptoundecanoic acid (CT-MUA) was performed using a protocol that was similar to that of CT-MHA. The first step involves protection of the thiol tail of MUA with a dimethoxytrityl (DMT) group to form the thioether MUA-DMT. Next, 1.09 g MUA were reacted with 1.76 g DMT-Cl and 0.84 mL of triethylamine in 50 mL of 5:4:1 tetrahydrofuran : acetic acid : water, at room temperature, under argon atmosphere, for 14 hr. MUA-DMT was

isolated and purified by silica column chromatography (3:1:1 hexane : ethyl ether : THF) yielding 1.3 g of a yellow/amber oil product.

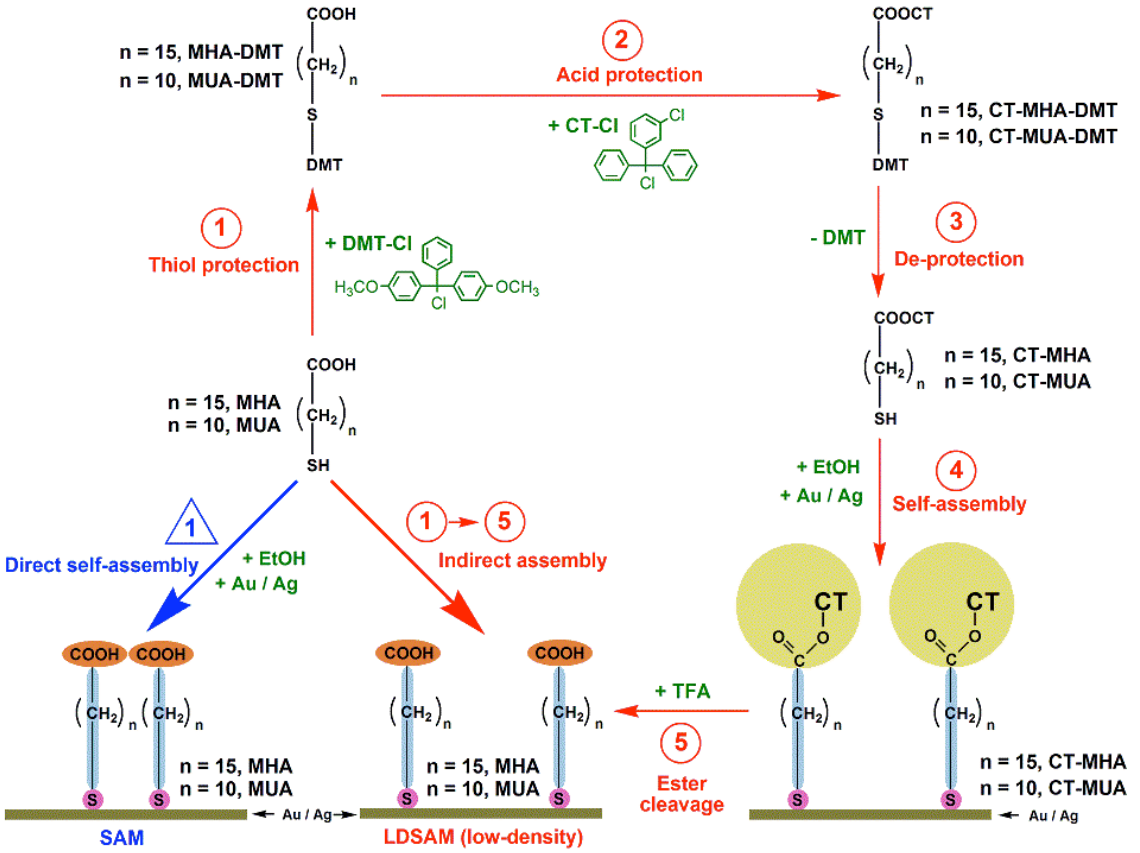

Figure 2. Preparation methods for traditional SAMs and LDSAMs. The formation of LDSAM's involves an indirect strategy via the CT ester, which consists of a bulky spacer group (from Peng et al., *Langmuir* 2007, included as attachment).

The second step involves protection of the carboxyl head group of MUA-DMT with a chlorotrityl (CT) group to form the ester/thioether CT-MUA-DMT. Next, 1.3 g of purified MUA-DMT were reacted with 0.91 g of CT-Cl and 0.91 mL of DIPEA in 50 mL methylene chloride, at room temperature, under argon atmosphere, for 14 hr. CT-MUA-DMT was isolated and purified by silica column chromatography (3:1 hexane : ethyl ether) yielding 0.68 g of a clear oil product. The third step involves de-protection of the DMT group from the thiol tail of MUA to form the ester CT-MUA. 0.68 g of purified CT-MUA-DMT was dissolved in 20 mL of 3:1 THF : methanol and 2 mL 1 M sodium acetate, to which was added a solution of 340 mg silver nitrate in 4 mL of 5:1 methanol : water. The mixture was stirred for 1 hr at room temperature. Precipitate was removed by centrifugation at 4000 × g for 5 minutes, followed by resuspension of the pellet in 15 mL of 3:1 THF : methanol, re-centrifugation at 4000 × g for 5 minutes, and combination of the two supernatants. A solution of 308 g of dithioerythritol (DTE) in 3 mL of 1 M sodium acetate was then added, and the mixture was stirred for 5 hr at room

temperature. Precipitate was removed by centrifugation at 4000 × g for 5 minutes, followed by resuspension of the pellet in 15 mL of 3:1 THF : methanol, re-centrifugation at 4000 × g for 5 minutes, and combination of the two supernatants. CT-MUA was isolated and purified by silica column chromatography (50 mL of 3:1 hexane : ethyl ether, followed by 1:1 hexane : ethyl ether), yielding 0.22 g of a clear oil product. CT-MUA (and CT-MHA) was aliquoted and stored at -20° C until used.

Detailed Analytical Data.

[MUA-DMT] ^{1}H NMR (300 MHz, $CDCl_3$) δ = 1.17-1.39 (m), 1.57-1.69 (m), 1.81-1.88 (m), 2.12-2.17 (t), 2.31-2.38 (t); 2.67-2.72 (t), 3.79 (s), 6.78-6.85 (m), 7.15-7.40 (m); ^{13}C NMR (100 MHz, $CDCl_3$) δ = 29.25, 29.40, 55.44, 113.23, 113.40, 127.99, 128.09, 129.08, 129.36, 129.64, 130.90, 132.35.

[CT-MUA-DMT] ^{1}H NMR (300 MHz, $CDCl_3$) δ = 1.17-1.29 (m), 1.62-1.69 (m), 1.79-1.88 (m) 2.12-2.17 (t), 2.31-2.37 (m), 2.66-2.71 (t) 3.34 (s), 3.74-3.80 (m), 3.90 (s), 3.95-3.99 (m) 6.69-6.85 (m) 6.94-6.99 (m) 7.08-7.60 (m) 7.74-7.86 (m); ^{13}C NMR (75 MHz, $CDCl_3$) δ = 24.92, 25.83, 28.67, 29.18, 29.38, 29.55, 34.20, 39.52, 55.45, 55.74, 55.99, 68.19, 82.82, 113.25, 113.39, 113.80, 115.01, 116.24, 126.63, 127.61, 127.98, 128.23, 128.43, 129.34, 129.65, 129.99, 130.90, 131.58, 131.72, 132.16, 132.84, 137.77, 143.93, 145.75, 179.63.

[CT-MUA] ^{1}H NMR (300 MHz, $CDCl_3$) δ = 1.10 - 1.35 (m), 1.56-1.68 (m), 1.95-2.00 (t), 2.31-2.36 (t), 7.17-7.35 (m), 7.43-7.46 (m); ^{13}C NMR (75 MHz, $CDCl_3$) δ = 24.92, 25.83, 28.67, 29.18, 29.38, 29.55, 34.20, 39.52, 52.68, 55.45, 55.74, 55.99, 68.19, 82.82, 113.25, 113.39, 113.80, 115.006, 116.243, 126.632, 127.611, 127.98, 128.23, 128.43, 129.34, 129.65, 129.99, 130.90, 131.58, 131.72, 132.16, 132.84, 137.77, 143.93, 145.75, 179.63. Electrospray mass spectrometry gave a mass-to-charge ratio of 517.1948 for the CT-MUA $[M+Na]^+$ adduct, consistent with a theoretical molar mass of 517.1944 g/mol calculated for the non-dimerized product.

Synthesis of molecular tweezers.

On a basis of a rational modeling approach we have identified promising initial structures for molecular tweezers and have worked towards a successful implementation of their synthesis. While initial synthesis efforts were challenging, we were able to establish a successful route recently (manuscript in preparation). While we are hopeful that this route can generate sufficient amounts of materials (gram scale) for our studies, we have so far only isolated analytical amounts of the end product. Further work will be directed towards repetition and refinement of the initial work to generate sufficient materials for the monolayer work proposed in Aimw #2 and #3.
Detaills of the synthesis are outlined below.

Cholic tetraol **2**: To a solution of cholic acid (16.4g, 97%) in anhydrous THF (300 mL) was carefully added $LiAlH_4$ (8.6 g, 95%). The resulting suspension was stirred at 50 °C under nitrogen for 24 hrs. After cooling in ice bath, the excess $LiAlH_4$ was quenched by careful addition of dilute HCl. 3 M HCl (600 mL) was added and the THF was then removed. After filtration, the solid crude product was washed with water and recrystallized from ethanol to give white crystals (14.5 g, 91%).

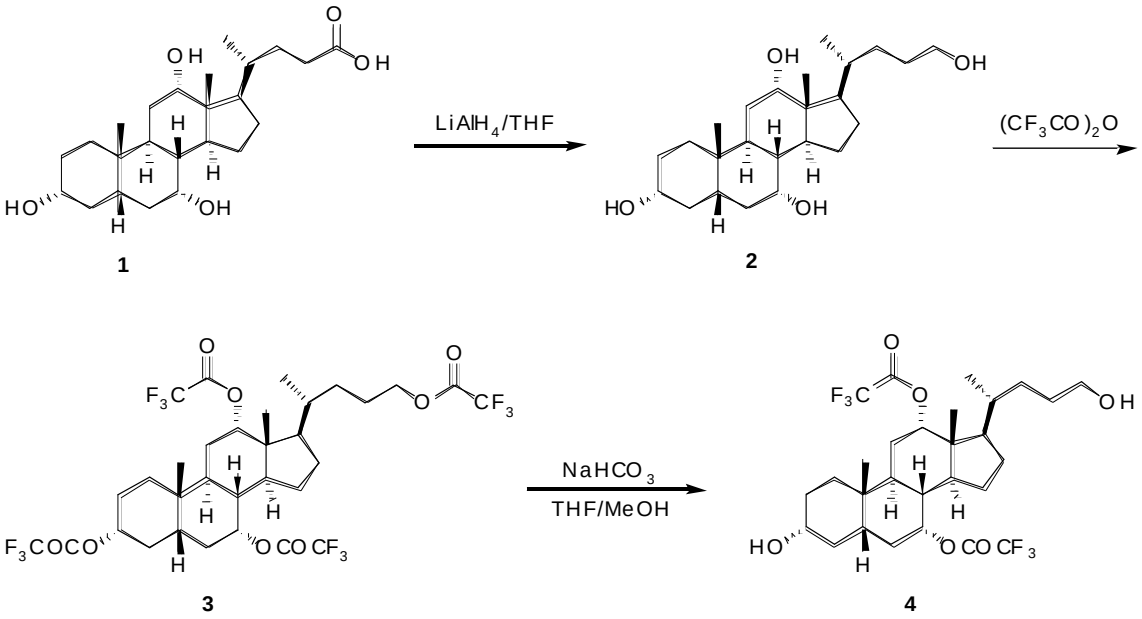

1 **2** **3** **4**

Cholic tetra-trifluoroacetate **3**: To a 250 mL round bottom flask cooled in ice bath charged with cholic tetraol **2** (9.1g) was added trifluoroacetic anhydride (60 mL) dropwise under nitrogen. After the addition, the solution was stirred at room temperature overnight. The volatile compounds were then removed under vacuum to give a colorless oil which was used without further purification.

Cholic di-trifluoroacetate **4:** To a cholic tetra-trifluoroacetate **3** solution in anhydrous THF (40 mL) was added anhydrous methanol (200 mL) and sodium

bicarbonate (10.0 g) and the resulting mixture was kept in refrigerator at 4 °C for 6 days.

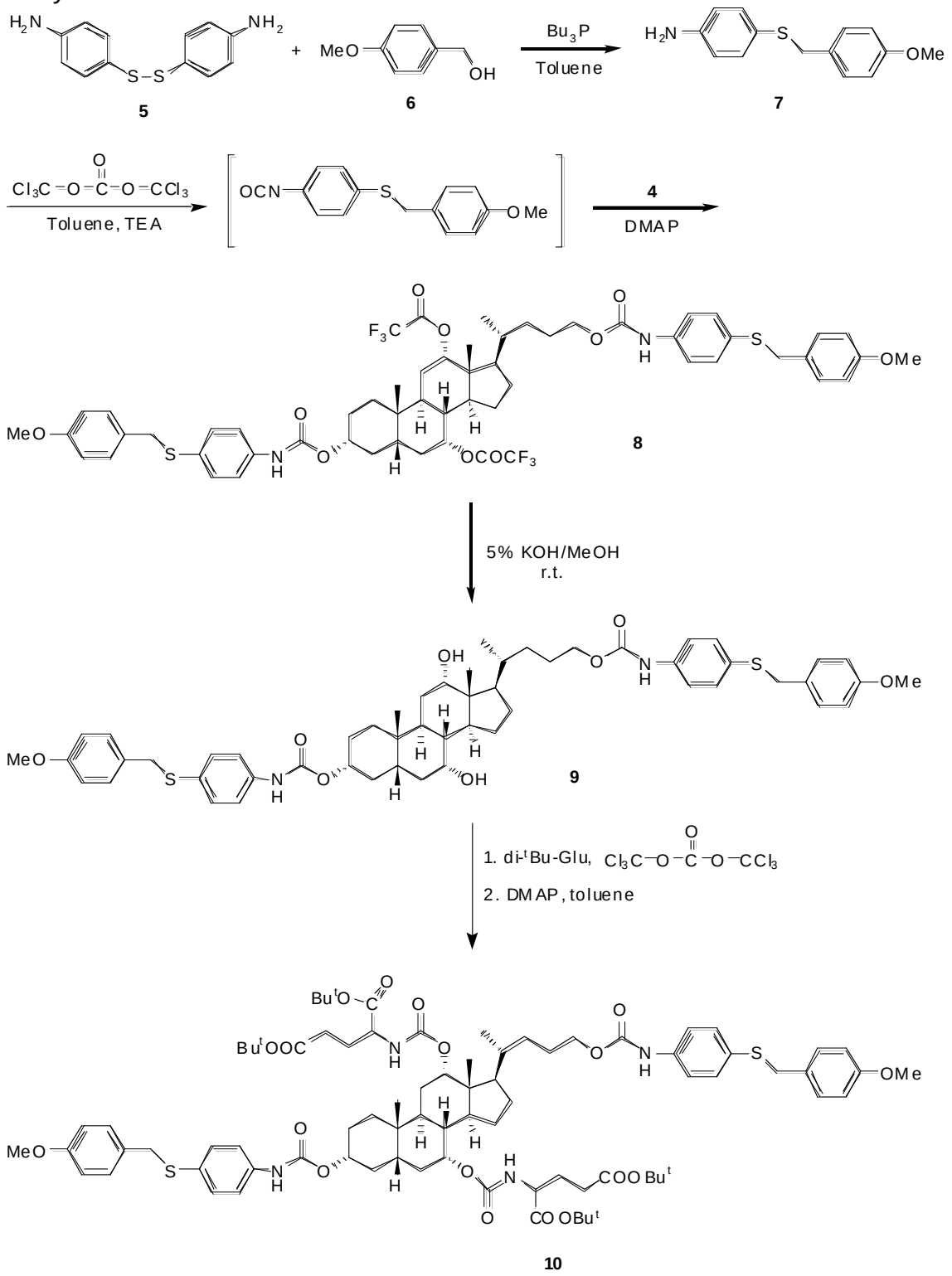

The reaction mixture was poured into ice water (500 mL) and extracted with ether (3 x 250 mL). The combined extracts was washed with brine (2 x 300 mL) and dried over Na_2SO_4. After filtration and removal of solvent, the pale yellow oil was purified on silica gel using hexanes/ethyl acetate (7/3, v/v) as eluent to give the product as a colorless solid.

Protected 4-aminophenyl thiol **7**: A solution of 4-aminophenyl disulfide **5** (5.3 g) and 4-methoxybenzyl alcohol **6** (2.2 mL) in anhydrous toluene (120 mL) was degassed by two freeze-pump-thaw cycles, followed by addition of tributylphosphine (5.0 mL) under argon and two more freeze-pump-thaw cycles. The mixture was then stirred at 70 °C under argon for 24 hrs. After cooling to room temperature, the reaction mixture was diluted with diethyl ether (200 mL), washed with 5 wt% aqueous NaOH (2 x 150 mL) and brine (2 x 150 mL), and dried over Na_2SO_4. After filtration and removal of solvents, the crude product was purified on silica gel using hexanes/ethyl acetate (7/3) as eluent to give the product as pale yellow crystals (3.9 g).

Cholic di-carbamate **8**: To a solution of protected 4-aminophenyl thiol **7** (3.5 g) in anhydrous toluene (60 mL) was added bis(trichloromethyl) carbonate (1.75 g). The resulting solution was refluxed under argon for three hours and then cooled to room temperature. Cholic di-trifluoroacetate **4** (3.8 g) was added into this cooled solution under argon purge and the solution was stirred at 60 °C under argon overnight. The reaction mixture was then cooled to room temperature, diluted with diether ether (300 mL), washed with 2 M HCl (3 x 50 mL) and brine (2 x 100 mL), and dried over Na_2SO_4. After filtration and removal of solvents, the residue was purified on silica gel using hexanes/EtOAc (65/35, v/v) as eluent to give the product as a pale yellow solid (4.8 g).

Cholic diol **9**: To a solution of NaOH (5.0 g) in methanol (150 mL) was added a solution of cholic di-carbamate **8** (5.4 g) in THF (30 mL). The resulting solution was stirred for 12 hours at room temperature, followed by the addition of 10 mL acetic acid. The solution was then poured into 400 mL of water and extracted with diethyl ether (3 x 250 mL). The combined ether layer was dried over Na_2SO_4. Filtration and removal of solvent gave crude product as a light brown oil which was purified on silica gel using hexanes/EtOAc (3/2, v/v) to give the product as white solid (4.2 g).

Cholic tetracarbamate **10**: To a solution of L-Glutamic acid di-*tert*-butyl ester hydrochloride (1.52 g) in anhydrous toluene (10 mL) cooled at – 80 °C was added triethylamine (2.1 mL) and a bis(trichloromethyl) carbonate (530 mg) solution in anhydrous toluene (4 mL) under nitrogen. The solution was allowed to slowly warm up to room temperature and stirred at RT for 4 hours. A cholic diol **9** (750 mg) solution in anhydrous toluene (10 mL) and anhydrous pyridine (4.5 mL) were then added into the reaction mixture using a syringe and the mixture was refluxed for 36 hours under nitrogen. After cooling to RT, the solution was diluted by diethyl ether (150 mL), washed with 2 M HCl (2 x 100 mL) and brine (2 x 100

mL), and dried over Na_2SO_4. After filtration and removal of solvents, the residue was purified on silca gel using CH_2Cl_2/ether (95/5, v/v) as eluent to give the product as a light brown oil (140 mg).

WORK DONE TOWARDS SPECIFIC AIM #2:

PREPARATION AND CHARACTERIZATION OF SMART SCREENING PLATFORMS FOR MODEL BIOINDICATORS.

Self-assembly of monolayers has been conducted so far with linear switches only and has been recently reported. The self-assembly of molecular tweezers will follow the approach described herein and the lessons learnt from the characterization of linear switches will equally apply to molecular tweezers.

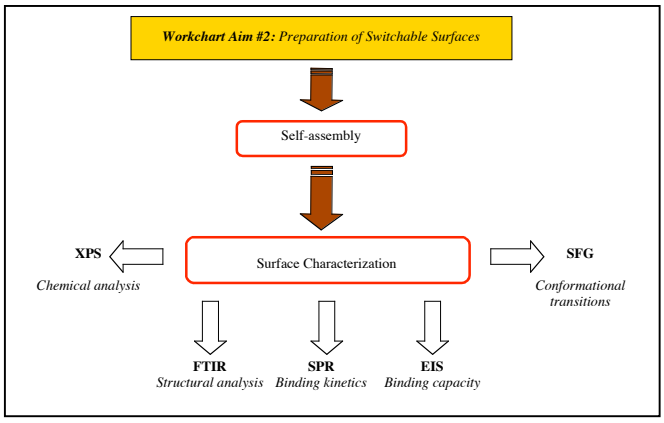

Monolayers of mercaptohexadecanoic acid and mercaptoundecanoic acid were assembled on both, gold and silver electrodes. When conducting electrochemical impedance spectroscopy under physiological conditions, these monolayers exhibit significant changes in their electrochemical barrier properties upon application of electrical DC potentials below +400 mV with respect to a standard calomel electrode. We further found the impedance switching to be reversible under physiological conditions. Moreover, the impedance can be fine-tuned by changing the magnitude of the applied electrical potential. Before and during impedance switching at pH 7.4 in aqueous buffer solutions, the low-density monolayers showed good stability according to grazing angle infrared spectroscopy data.

Further details of the synthesis and characterization via FTIR and impedance spectroscopy have been reported in a recent publication and have been included as attachment.

In an extension of these initial studies, we have examined the storage stability of monolayers made of linear molecular switches for several weeks. Extended stability is an important criterion for selection of suitable signal transduction systems. A manuscript describing the stability is currently under preparation will be submitted to Langmuir within a month.

Microfabrication methods have been used to produce substrates appropriate for monolayer analysis techniques such as electrochemical impedance spectroscopy, as shown in Figure 3. These substrates consisted of a 4500 Å SiO_2 insulating layer, a 100 Å titanium adhesive layer, and a 1000 Å gold active

layer. The electrical contacting zone allows connection of an electrical lead to the monolayer zone (via the conductive strip). The monolayer zone is of a defined surface area (2.5 cm^2), for controlled measurement of electrochemical parameters that scale with surface area. Root mean square roughness of gold surfaces has been determined by atomic force microscopy to be <2 nm, providing an ultra-flat surface for monolayer assembly. The gold substrate have been prepared by rinsing with copious amounts of absolute ethanol, deionized water, and absolute ethanol. Substrates have been dried under a stream of nitrogen. The monolayer have been formed by immersing the gold substrate into a solution of the precursor following well-characterized protocols.[5,6,7] After rinsing away unadsorbed molecules with ethanol/water/ethanol and drying under nitrogen, the quality of the monolayers have been assessed by a combination of surface-sensitive analytical methods including grazing angle FTIR, X-ray photoelectron spectroscopy, contact angle measurements, ellipsometry, cyclic voltammetry, and electrochemical impedance spectroscopy, and sum frequency generation spectroscopy.

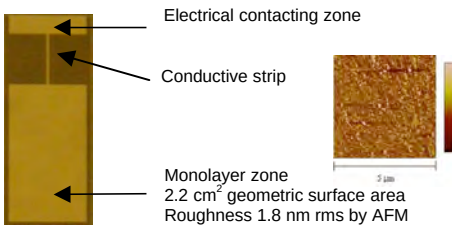

Fig. 3. *Microfabricated gold electrodes used for self-assembly studies (inlet: AFM image of the gold surface).*

Electrochemical Impedance Spectroscopy (EIS) was performed using a standard 3-electrode electrochemical cell (SAM sample as working electrode, saturated standard calomel electrode [SCE] as reference electrode, and platinum mesh as counter electrode) with N_2-purged phosphate buffered saline as electrolyte solution. A Gamry PCI4/300 potentiostat with EIS300 software module was used to take EIS measurements. The applied potential had an AC amplitude of 10 mV r.m.s. and a frequency range from 1 Hz to 10^5 Hz, with a DC bias of 0 mV w.r.t. SCE. The amplitude and phase angle of the current response were recorded at ten points per decade in frequency. Data for samples measure at regular intervals during 1 month are shown in Figure 4. For both, high-density and low-density monolayers, impedance did not show significant decrease over the 4 week window suggesting outstanding stability of the monolayers under the selected storage conditions. This data are important for further use of Self-assembled Monolayers of linear molecular switched in breath analyzer devices for breast cancer.

Moreover, the same samples were subjected to structural analysis using FTIR. Fourier Transform Infrared (FTIR) Spectroscopy was performed using a liquid-nitrogen-cooled Thermo Nicolet 6700 spectrometer in 85° grazing angle mode with a 16 mm aperture. At least 128 scans were taken per sample at 4 cm^{-1} resolution. Data of the symmetric and asymmetric CH stretches are shown in Figures 5 and 6 for both high and low density monolayers of linear molecular switches. A shift in the peak position indicated structural reorientations. On the basis of the FTIR data, a time-dependent reorientation of the low-density

monolayers, but not the high-density monolayers can be proposed. This appears somewhat surprising in the light of the impedance data, which suggest consistent stability over the entire time course. Impedance spectroscopy is extremely sensitive to pinhole defects.

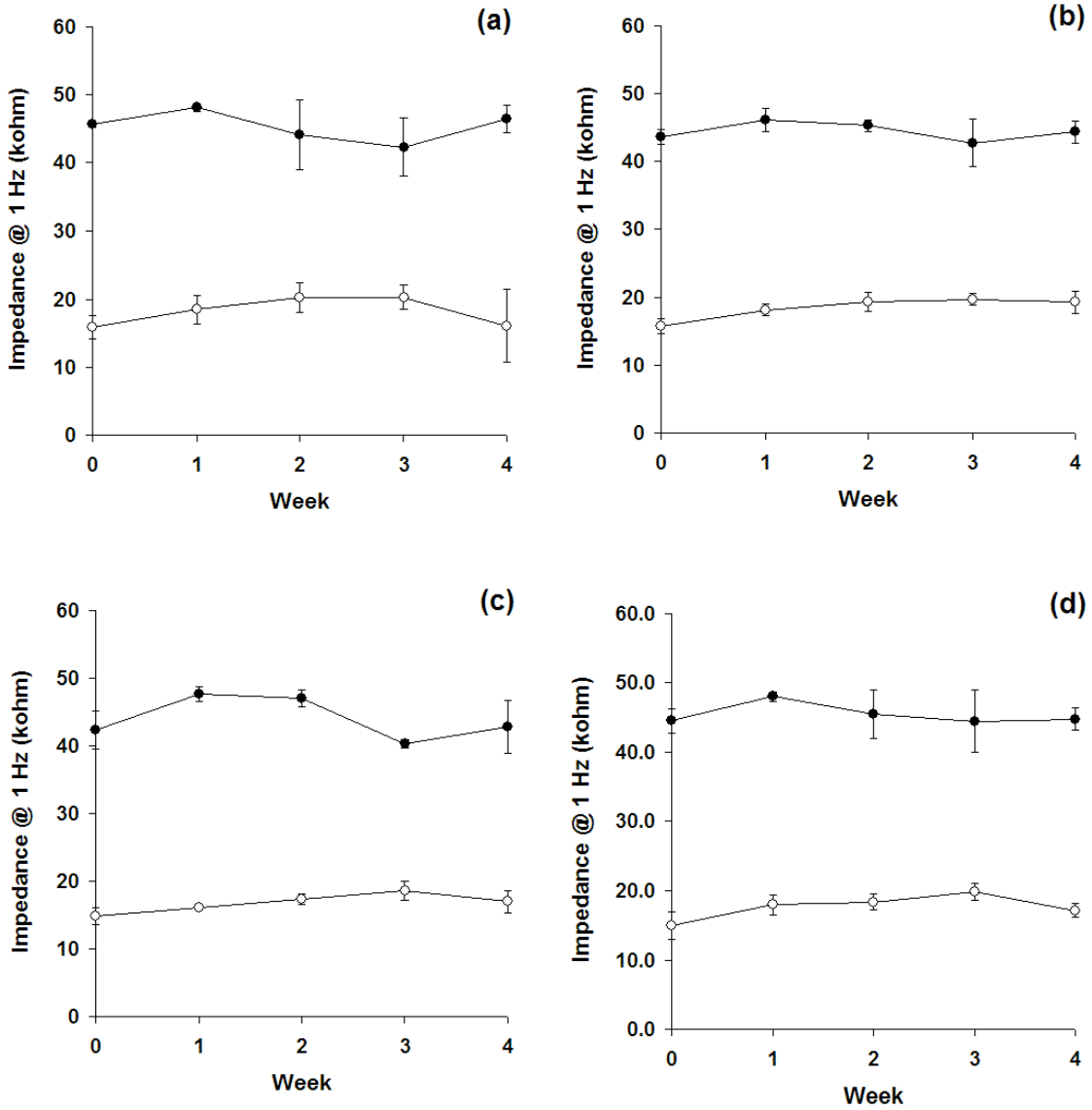

Figure 4. *Impedance modulus at 1 Hz of high-density SAMs (solid circles) and low-density SAMs (open circles) stored under various conditions. (a) 20° C under air (b) 20° C under argon, (c) 4° C under argon, (d) 20° C under ethanol.*

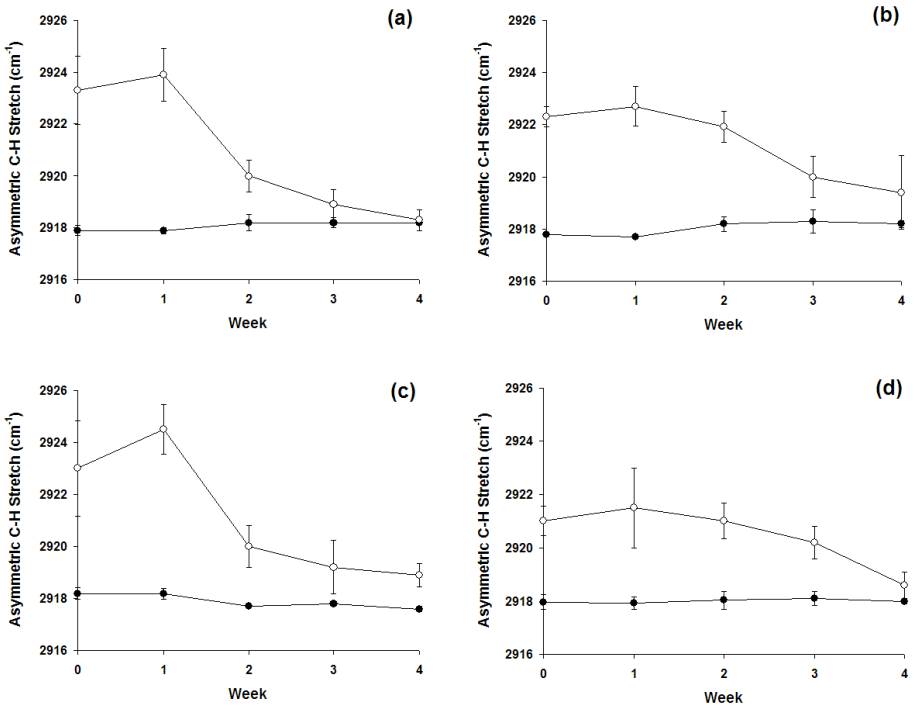

Figure 5. *FTIR peak locations for the asymmetric C-H stretch of high-density SAMs (solid circles) and low-density SAMs (open circles) stored under various conditions. (a) 20° C under air (b) 20° C under argon, (c) 4° C under argon, (d) 20° C under ethanol.*

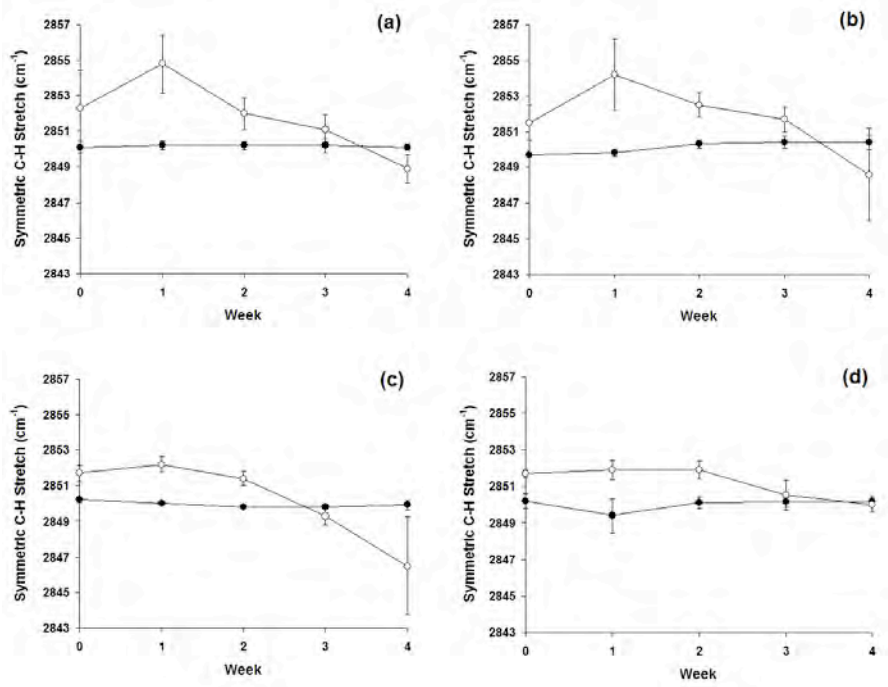

Figure 6. *FTIR peak locations for the symmetric C-H stretch of high-density SAMs (solid circles) and low-density SAMs (open circles) stored under various conditions. (a) 20° C under air (b) 20° C under argon, (c) 4° C under argon, (d) 20° C under ethanol.*

To further investigate this apparent inconsistency, we also studied to chemical stability of high density and low-density monolayers of linear molecular switches. If a chemical degradation of the monolayer occurred, the sulfur that tethers the molecular switches to the gold electrode would be oxidized resulting in a detectable shift in the S2p spectrum shown in Figure 7. X-ray photoelectron spectroscopy (XPS) was performed using an Axis Ultra (Kratos Analyticals, UK) instrument equipped with a monochromatized AlKα X-ray source. Spectra were normalized with respect to aliphatic carbon at 285.0 eV. Within the margins of error, the S2p did not change throughout the observation period confirming the impedance data that suggest high stability and fidelity of the surfaces over several weeks of storage. Why a reorientation within the monolayer occurs and the importance of this effect on switching and diagnostics in unclear at this point, but will be a focus of further studies. Especially, if we start working with the molecular tweezers, we will reevaluate the apparent discrepancy between Impedance spectroscopy, XPS on the one hand, and FTIR on the other.

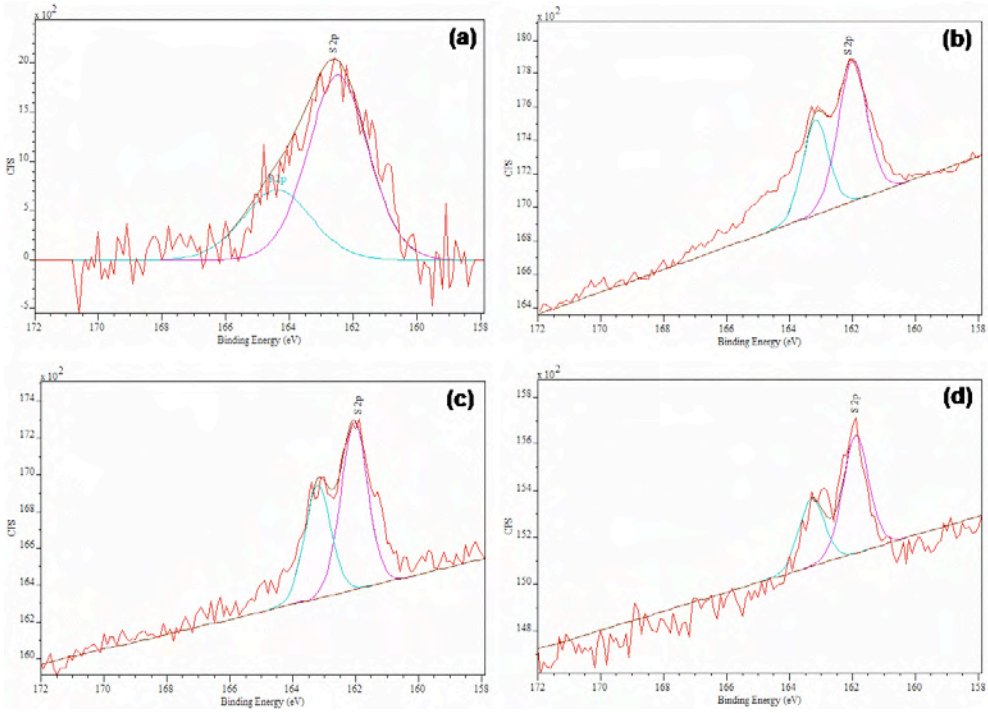

Figure 7. High resolution S 2p XPS spectra of low-density SAMs. (a) before storage (b) after 4 weeks at 20° C under air (c) after 4 weeks at 20° C under argon, (d) after 4 weeks at 4° C under argon.

C. KEY RESEARCH ACCOMPLISHMENTS

- Two different types of linear molecular switches have been identified, synthesized, characterized and sufficient quantities have been prepared for further studies. These molecules will be used as signal transduction units in future breast cancer detection devices.

- One type of molecular switch has been designed by a rationale approach and has subsequently synthesized in a multi-step synthesis. Analytical amounts have been already prepared and the characterization of the molecular tweezers and some of the molecular precursors has been mostly accomplished. However, the material synthesized in the first approach is still not sufficient for assembly in monolayers and the synthesis will be repeated to ensure sufficient materials.

- Low-density monolayers have been prepared on the basis of the linear molecular switches and the resulting monolayers have been fully characterized by FTIR, XPS, and ellipsometry.

- Silver has been established as an alternative electrode material to gold, which has the promise of cost benefits during integration and translational deployment.

- Switching of two monolayers has been demonstrated on the basis of impedance spectroscopy. The fact that switching correlates with a change in impedance is a critical feature of the system because it allows for convenient monitoring of the surfaces AND detection of analytes in the later phase of the project.

- Monolayers were demonstrated to not only undergo binary switching, but the be tunable by a transient application of small electrical potentials. Another important property, when considering use of linear molecular switches as signal transduction systems for breast cancer analysis.

- The storage stability of self-assembled monolayers of linear molecular switches has been demonstrated over a period of 4 weeks. Storage stability is an important criterion for translational deployment.

- A collaboration with Daniel F. Hayes, M.D., who is the Clinical Director, Breast Oncology Program at the University of Michigan Comprehensive Cancer Center, has been initiated. This collaboration will be critical with respect to initial discussions and guidance regarding medical practice and focus on the right targets. In long term, we intend to engage in true translational activities jointly with Dr. Hayes.

D. REPORTABLE OUTCOMES

a. Work sponsored under this proposal (Aim #1 and #2) has resulted in a **full paper**, which appeared in January 2007 in a special issue of Langmuir, which described major contributions in the area of smart materials. The paper is included as attachment. The paper represents a major article and was solicited as an invited contribution. The publication had several co-authors including graduate and undergraduate students.

b. Work sponsored under this proposal (Aim #1 and #2) has resulted in **one oral presentation** at the Annual Meeting of the American Institute of Chemical Engineers. The work was presented by David Peng, a leading graduate student in this program.

c. A second **publication** on the stability of surfaces made of linear molecular switches is currently **under preparation**.

d. A **keynote lecture** on smart systems entitled “Materials that enable smart properties” was delivered during the Annual German American Frontiers of Engineering Meeting sponsored by the National Academy of Engineering.

e. The following list includes selected **invited seminars** were delivered that reported on work sponsored under this grant.

2006 J. Lahann, Engineering Biointerfaces with Controlled Properties, Annual Meeting of the German Society of Biomaterials, Essen.

2006 J. Lahann, Engineering Biointerfaces with Controlled Properties, University of Michigan Medical School, Department of Internal Medicine.

2006 J. Lahann, Engineering Biointerfaces with Controlled Properties, Bio 2006, Chicago.

2006 J. Lahann, Engineering Biointerfaces with Controlled Properties, Laval University.

2006 J. Lahann, Engineering Biointerfaces with Controlled Properties, University of Southern Mississippi.

2006 J. Lahann, Engineering Biointerfaces with Controlled Properties, ACS Central Regional Meeting Frankenmuth, MI.

2006 J. Lahann, Designer Materials: Engineering Biointerfaces with Controlled Properties, European Coatings Conference "Smart

Coatings V", Berlin, Germany.

2006 *J. Lahann, Engineering Biointerfaces with Controlled Properties, University of Aachen (RWTH), Germany.*

D. CONCLUSION

During the first year of this three-year program we have made considerable progress. We have finished work proposed under Aim #1 and have made significant progress towards completion of Aim #2. The work with linear molecular switches has been already completed and we have established the tools and methods to finalize the work with molecular tweezers, as soon as sufficient quantities have been synthesized. In spite of the high-risk character of the project, the progress is in line with the initially proposed timeline. So far, no major adjustment has been necessary, but several critical challenges, such as binding of analytes to the sensor surface or rechargeability of the surfaces, will be faced in the next year and adjustments will be more likely to be encountered during this period. A small but important adjustment was the study of storage stability of the low-density monolayers of linear molecular switches, which addresses a practically important concern for future applications in breast cancer detection.

E. REFERENCES

[1] D.K. Peng, S.T. Yu, D.J. Alberts, J. Lahann, Switching the Electrochemical Impedance of Low-Density Self Assembled Monolayers, *Langmuir* **2007**, 23, 297-304.

[2] Love, J.C.; Estroff, L.A.; Kriebel, J.K.; Nuzzo. R.G.; Whitesides G.M. *Chem. Rev.* **2005**, *105*, 1103-1169.

[3] a) Schreiber, F. *J. Phys.: Condens. Matter* **2004**, *16*, R881-R900; b) Schwartz, D.K. *Annu. Rev. Phys. Chem.* **2001**, *52*, 107-137; c) Ulman, A. *Chem. Rev.* **1996**, *96*, 1533-1554.

[4] Lahann, J.; Mitragotri, S.; Tran, T.N.; Kaido, H.; Sundaram, J.; Choi, I.S.; Hoffer, S.; Somorjai, G.A.; Langer, R. *Science* **2003**, *299*, 371-373.

[5] R. G. Nuzzo, D. L. Allara, "Adsorption of Bifunctional Organic Disulfides on Gold Surfaces," *Journal of the American Chemical Society*, **105**, 4481, 1983.

[6] A. Ulman, "Formation and Structure of Self-Assembled Monolayers," *Chemical Reviews*, **96**, 1533, 1996.

[7] D. K. Schwartz, "Mechanisms and Kinetics of Self-Assembled Monolayer Formation," *Annual Review of Physical Chemistry*, **52**, 107, 2001.

Switching the Electrochemical Impedance of Low-Density Self-Assembled Monolayers†

David K. Peng, Sandy T. Yu, David J. Alberts, and Joerg Lahann*

Department of Chemical Engineering, University of Michigan, 2300 Hayward Street, Ann Arbor, Michigan 48105

Received June 12, 2006. In Final Form: August 16, 2006

Because the active remodeling of biointerfaces is a paramount feature of nature, it is very likely that future, advanced biomaterials will be required to mimic at least certain aspects of the dynamic properties of natural interfaces. This need has fueled a quest for model surfaces that can undergo reversible switching upon application of external stimuli. Herein, we report the synthesis and characterization of a model system for studying reversibly switching surfaces based on low-density monolayers of mercaptohexadecanoic acid and mercaptoundecanoic acid. These monolayers were assembled on both gold and silver electrodes. When conducting electrochemical impedance spectroscopy under physiological conditions, these monolayers exhibit significant changes in their electrochemical barrier properties upon application of electrical DC potentials below +400 mV with respect to a standard calomel electrode. We further found the impedance switching to be reversible under physiological conditions. Moreover, the impedance can be fine-tuned by changing the magnitude of the applied electrical potential. Before and during impedance switching at pH 7.4 in aqueous buffer solutions, the low-density monolayers showed good stability according to grazing angle infrared spectroscopy data. We anticipate low-density monolayers to be potentially useful model surfaces when designing active biointerfaces for cell-based studies or rechargeable biosensors.

Introduction

Although great progress has been made over the past decade in the development of passive cell substrates for biomedical applications,[1−5] future research will need to address the intrinsically static character of such artificial substrates and the functional limitations encountered due to the lack of active, dynamic biomaterial properties.[5,6] At the cell−extracellular matrix (ECM) interface, both cell receptors and ECM proteins undergo rapid, dynamic remodeling.[7−10] This active remodeling of the biointerface is a critical feature of natural ECM, and the design of next-generation biomaterials must account for the dynamic aspects of these interfaces. The need for substrates that can dynamically regulate biological functions such as cell adhesion, proliferation, and differentiation has recently led to a variety of "smart material" designs in which control of biomaterial properties is stimulated by changes in temperature or pH or via light-induced or electrochemical modifications.[11−23] Herein, we report studies on a new class of smart materials—low-density self-assembled monolayers, or LDSAMs—which can undergo reversible conformational transitions that dynamically change the macroscopic surface properties of the monolayers.[23,24] Unlike traditional self-assembled monolayers (SAMs), which assemble in tightly packed arrangements, LDSAMs show increased conformational freedom of their constituent alkanethiolate molecules, which allows LDSAMs to exhibit unique, reversible responsiveness to the application of electrical potential.[23]

Although a range of surface analysis methods are available for characterization of switchable surfaces—including infrared spectroscopy, X-ray photoelectron spectroscopy (XPS), surface plasmon spectroscopy, ellipsometry, sum frequency generation spectroscopy, and cyclic voltammetry (CV)—electrochemical impedance spectroscopy (EIS) has become an increasingly important tool for SAM analysis. This trend is seen mainly because of the precise surface-sensitive analytical information that electrochemical methods provide and because of the small (∼10 mV) sinusoidal probe voltages that are used in EIS, which make it a less perturbing method than CV.

Studies of the electrical properties of SAMs by EIS can be divided into those that examine electronic conduction through SAMs using redox-active probes and those that follow the ionic conduction through SAMs using solution ions in the absence of redox probes. The majority of the EIS studies on SAMs reported in the literature have been conducted using redox probes, which has enabled studies of a variety of important characteristics of SAMs.[25−36] For instance, studies have examined the growth

† Part of the Stimuli-Responsive Materials: Polymers, Colloids, and Multicomponent Systems special issue.

* To whom correspondence should be addressed. E-mail: lahann@umich.edu.

(1) Stevens, M. M.; George, J. H. *Science* **2005**, *310*, 1135−1138.
(2) Lutolf, M. P.; Hubbell, J. A. *Nat. Biotechnol.* **2005**, *23*, 47−55.
(3) Vogel, V.; Baneyx, G. *Annu. Rev. Biomed. Eng.* **2003**, *5*, 441−63.
(4) Mrksich, M. *Curr. Opin. Chem. Biol.* **2002**, *6*, 794−797.
(5) Lahann, J.; Langer, R. *MRS Bull.* **2005**, *30*, 185−188.
(6) Stupp, S. I.; Donners, J. J. J. M.; Li, L. S.; Mata. A. *MRS Bull.* **2005**, *30*, 864−873.
(7) Holmbeck, K.; Szabova, L. *Birth Defects Res. C Embryo Today* **2006**, *78*, 11−23.
(8) Midwood, K. S.; Williams, L. V.; Schwarzbauer, J. E. *Int. J. Biochem. Cell Biol.* **2004**, *36*, 1031−1037.
(9) Brown, L. *Am. J. Physiol. Heart Circ. Physiol.* **2005**, *289*, H973−974.
(10) Davis, G. E.; Senger, D. R. *Circ. Res.* **2005**, *97*, 1093−1107.
(11) de las Heras Alarcon C.; Pennadam, S.; Alexander, C. *Chem Soc. Rev.* **2005**, *34*, 276−285.
(12) Kikuchi, A.; Okano, T. *J. Controlled Release* **2005**, *101*, 69−84.
(13) Tsuda, Y.; Kikuchi, A.; Yamato, M.; Sakurai, Y.; Umezu, M.; Okano, T. *J. Biomed. Mater. Res. A* **2004**, *69*, 70−78.
(14) Riskin, M.; Basnar, B.; Chegel, V. I.; Katz, E.; Willner, I.; Shi, F.; Zhang, X. *J. Am. Chem. Soc.* **2006**, *128*, 1253−1260.
(15) Wang, X.; Kharitonov, A.; Katz, E.; Willner, I. *Chem. Commun.* **2003**, *9*, 1542−1543.
(16) Jeong, B.; Gutowska, A. *Trends Biotechnol.* **2002**, *20*, 305−311.
(17) Russell, T. P. *Science* **2002**, *297*, 964−967.
(18) Liu, Y.; Mu, L.; Liu, B. H.; Zhang, S.; Yang, P. Y.; Kong, J. L. *Chem. Commun.* **2004,** *10*, 1194−1195.
(19) Abbott, S.; Ralston, J.; Reynolds, G.; Hayes, R. *Langmuir* **1999**, *15*, 8923−8928.
(20) Ichimura, K.; Oh, S. K.; Nakagawa, M. *Science* **2000**, *288*, 1624−1626.
(21) Abbott, N. L.; Gorman, C. B.; Whitesides, G. M. *Langmuir* **1995**, *11*, 16−18.
(22) Chi, Y. S.; Lee J. K.; Lee, S. G.; Choi, I. S. *Langmuir* **2004**, *20*, 3024−3027.
(23) Lahann, J.; Mitragotri, S.; Tran, T. N.; Kaido, H.; Sundaram, J.; Choi, I. S.; Hoffer, S.; Somorjai, G. A.; Langer, R. *Science* **2003**, *299*, 371−373.
(24) Katz, E.; Lioubashevsky, O.; Willner, I. *J. Am. Chem. Soc.* **2004**, *126*, 15520−15532.

10.1021/la061677o CCC: $37.00
Published on Web 10/26/2006

properties of dodecaneselenol,[26] octadecanethiol,[27] and naphthalene disulfide[28] monolayers, determining the relative time scales for monolayer adsorption and reorganization/crystallization; electron-transfer kinetics have been examined for dodecanethiol[29] and 4′-hydroxy-4-mercaptobiphenyl[30,31] monolayers; and monolayer pinhole size and separation have been studied for octadecanethiol monolayers.[32] Redox probe studies have also examined the passivation of a gold surface by 2-mercapto-3-*n*-octylthiophene,[33] the fractional coverage of octadecanethiol molecules,[34] and the change in the electrical "apparent thickness" of alkanethiol monolayers.[35]

In solutions without redox couples, ionic permeability through the monolayers plays the dominant role in the conduction of current. This phenomenon has been used to study acid−base reactions for mercaptohexadecanoic acid (MHA) and mercaptododecylamine monolayers,[37] the ionic insulating properties of alkanethiol monolayers of different chain lengths,[38,39] the effect of applied potential on alkanethiol monolayer structure,[40] the potential-induced desorption of monolayers,[41] and the insulating properties of adsorbed protein layers on alkanethiol monolayers.[42] The studies of Boubour and Lennox[39−41] in particular have presented a number of observations that suggest the usefulness of redox-inactive EIS for studying ionic permeability of low-density monolayers. First, well-packed SAMs, which exhibit strong barriers to ionic penetration, typically display low-frequency (1 Hz < f < 1000 Hz) phase angles approaching 90° (the theoretical phase angle for an ideal capacitor). In contrast, SAMs that display low-frequency phase angles below 87° show current leakage at pinholes and grain boundaries. Second, only in the medium-to-high-frequency range (100 Hz and up) does a change in electrolyte composition (e.g., salt concentration) affect the impedance trace. Third, upon the application of DC potential greater than a certain critical potential, the monolayer structure is perturbed and ionic permeability increases significantly, as long as potential-induced desorption can be excluded.

Despite the usefulness of redox probes for the determination of monolayer properties, practical concerns, particularly when pursuing biological or biomedical applications, will require far different environments from those seen in a typical electrochemical cell containing soluble hexaferrocyanide/hexaferricyanide. For this reason, the EIS measurements taken during these studies were performed in phosphate-buffered saline (PBS), an inert, redox-inactive, and physiologically relevant electrolyte solution. Our findings show that this analytical setup can be used to make accurate distinctions between different SAM types that are structurally very similar, and the aforementioned studies also provide a precedent for the study of purely ionic conductance through SAMs in the absence of redox couples.[39−41]

Although the physicochemical properties of a range of different SAMs have been studied extensively,[25,43−46] these studies have been limited to traditional dense SAMs, which do not exhibit tunable responsiveness to dynamic stimuli. Here we extend this method to LDSAMs assembled on gold and silver.

Experimental Section

Materials. MHA, mercaptoundecanoic acid (MUA), hexadecanethiol (HDT), undecanethiol (UDT), dimethoxytrityl chloride (DMT-Cl), triethylamine (TEA), diisopropylethylamine (DIPEA), absolute ethanol, and PBS were purchased from Sigma Aldrich (St. Louis, MO). Chlorotrityl chloride (CT-Cl) was purchased from TCI America (Portland, OR). Chemicals were used as received. Deionized water was produced using a Barnstead International (Dubuque, IA) E-pure system. Prime grade silicon wafers were purchased from Silicon Valley Microelectronics (Santa Clara, CA). Gold, silver, and titanium (99.99+%) were purchased from Alfa Aesar (Ward Hill, MA).

Synthesis of 16-Chlorotrityl-mercaptohexadecanoic Acid (CT-MHA) and 16-Chlorotrityl-mercaptoundecanoic Acid (CT-MUA). The synthesis of 16-chlorotrityl-mercaptohexadecanoic acid (CT-MHA) has been reported previously.[23] The synthesis of 16-chlorotrityl-mercaptoundecanoic acid (CT-MUA) was performed using a protocol that was similar to that of CT-MHA. The first step involves protection of the thiol tail of MUA with a dimethoxytrityl (DMT) group to form the thioether MUA-DMT. Next, 1.09 g of MUA was reacted with 1.76 g of DMT-Cl and 0.84 mL of triethylamine in 50 mL of 5:4:1 tetrahydrofuran/acetic acid/water, at room temperature, under argon atmosphere, for 14 h. MUA-DMT was isolated and purified by silica column chromatography (3:1:1 hexane/ethyl ether/THF) yielding 1.3 g of a yellow/amber oil product. The second step involves protection of the carboxyl headgroup of MUA-DMT with a chlorotrityl (CT) group to form the ester/thioether CT-MUA-DMT. Next, 1.3 g of purified MUA-DMT was reacted with 0.91 g of CT-Cl and 0.91 mL of DIPEA in 50 mL methylene chloride at room temperature under argon atmosphere for 14 h. CT-MUA-DMT was isolated and purified by silica column chromatography (3:1 hexane/ethyl ether) yielding 0.68 g of a clear oil product. The third step involves deprotection of the DMT group from the thiol tail of MUA to form the ester CT-MUA. Purified CT-MUA-DMT (0.68 g) was dissolved in 20 mL of 3:1 THF/methanol and 2 mL of 1 M sodium acetate to which was added a solution of 340 mg of silver nitrate in 4 mL of 5:1 methanol/water. The mixture was stirred for 1 h at room temperature. Precipitate was removed by centrifugation at 4000*g* for 5 min, followed by resuspension of the pellet in 15 mL of 3:1 THF/methanol, recentrifugation at 4000*g* for 5 min, and combination of the two supernatants. A solution of 308 g of dithioerythritol (DTE) in 3 mL of 1 M sodium acetate was then added, and the mixture was stirred for 5 h at room temperature. Precipitate was removed by centrifugation at 4000*g* for 5 min, followed by resuspension of the pellet in 15 mL of 3:1 THF/methanol, recentrifugation at 4000*g* for 5 min, and combination of the two supernatants. CT-MUA was isolated and purified by silica column chromatography (50 mL of 3:1 hexane/ethyl ether, followed by 1:1 hexane/ethyl ether), yielding 0.22 g of a clear oil product. CT-MUA (and CT-MHA) was aliquoted and stored at −20° C until used. [MUA-DMT] ^{1}H NMR (300 MHz, $CDCl_3$) δ 1.17−1.39 (m), 1.57−1.69 (m), 1.81−1.88 (m), 2.12−2.17 (t), 2.31−2.38 (t); 2.67−2.72 (t), 3.79 (s), 6.78−6.85 (m),

(25) Love, J. C.; Estroff, L. A.; Kriebel, J. K.; Nuzzo. R. G.; Whitesides G. M. *Chem. Rev.* **2005**, *105*, 1103−1169.
(26) Protsailo, L. V.; Fawcett, W. R.; Russell, D.; Meyer, R. L. *Langmuir* **2002**, *18*, 9342−9349.
(27) Diao, P.; Jiang, D.; Cui, X.; Gu, D.; Tong, R.; Zhong, B. *J. Electroanal. Chem.* **1999**, *464*, 61−67.
(28) Bandyopadhyay, K.; Vijayamohanan, K.; Shekhawat, G. S.; Gupta, R. P. *J. Electroanal. Chem.* **1998**, 447, *1*, 11−16.
(29) Xing, Y. F.; O′Shea, S. J.; Li, S. F. Y. *J. Electroanal. Chem.* **2003**, *542*, 7−11.
(30) Janek, R. P.; Fawcett, W. R.; Ulman, A. *Langmuir* **1998**, *14*, 3011−3018.
(31) Janek, R. P.; Fawcett, W. R.; Ulman, A. *J. Phys. Chem. B* **1997,** *101*, 8550−8558.
(32) Diao, P.; Guo, M.; Tong, R. *J. Electroanal. Chem.* **2001**, *495*, 98−105.
(33) Peng, Z.; Dong, S. *Langmuir* **2001**, *17*, 4904−4909.
(34) Diao, P.; Guo, M.; Jiang, D.; Jia, Z.; Cui, X.; Gu, D.; Tong, R.; Zhong, B. *J. Electroanal. Chem.* **2000**, *480*, 59−63.
(35) Cui, X.; Jiang, D.; Diao, P.; Li, J.; Tong, R.; Wang, X. *J. Electroanal. Chem.* **1999**, *470*, 1, 9−13.
(36) Widrig, C. A.; Chung, C.; Porter, M. D. *J. Electroanal. Chem.* **1991**, *310*, 335−359.
(37) Schweiss, R.; Werner, C.; Knoll, W. *J. Electroanal. Chem.* **2003**, *540*, 145−151.
(38) Protsailo, L. V.; Fawcett, W. R. *Langmuir* **2002**, *18*, 8933−8941.
(39) Boubour, E.; Lennox, R. B. *Langmuir* **2000**, *16*, 4222−4228.
(40) Boubour, E.; Lennox, R. B. *J. Phys. Chem. B* **2000**, *104*, 9004−9010.
(41) Boubour, E.; Lennox, R. B. *Langmuir* **2000**, *16*, 7464−7470.
(42) Bordi, F.; Prato, M.; Cavalleri, O.; Cametti, C.; Canepa, M.; Gliozzi, A. *J. Phys. Chem. B* **2004**, *108*, 20263−20272.
(43) Schreiber, F. *J. Phys.: Condens. Matter* **2004**, *16*, R881−R900.
(44) Schwartz, D. K. *Annu. Rev. Phys. Chem.* **2001**, *52*, 107−137.
(45) Ulman, A. *Chem. Rev.* **1996**, *96*, 1533−1554.
(46) Dubois, L. H. *Annu. Rev. Phys. Chem.* **1992**, *43*, 437−463.

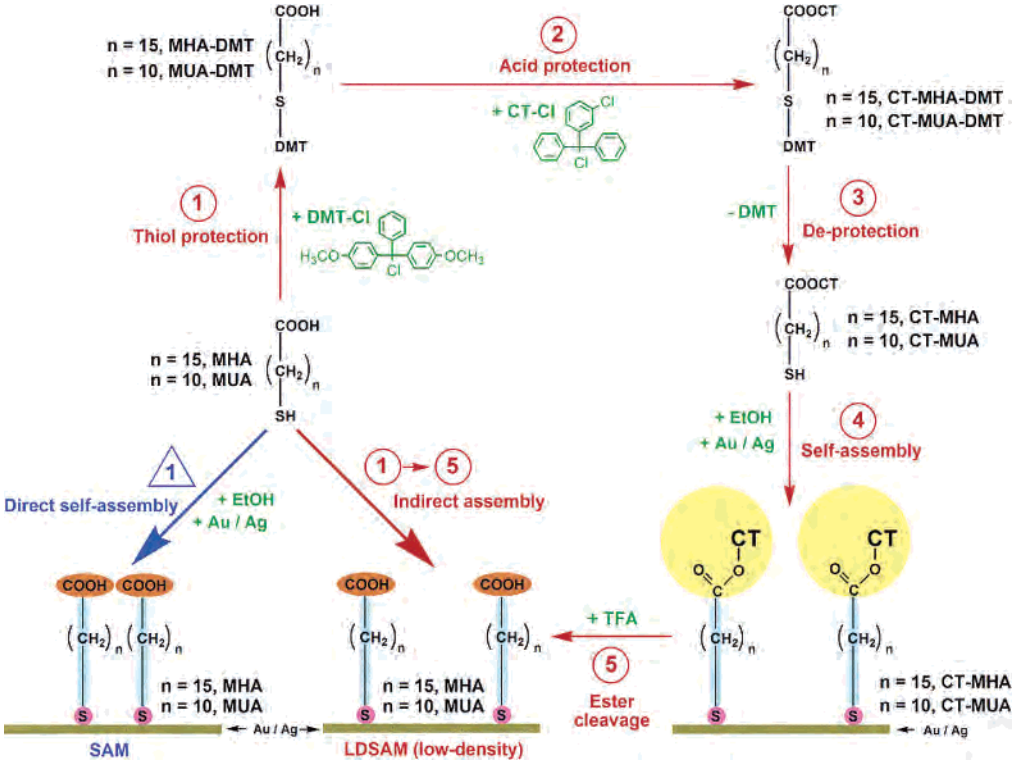

Figure 1. Preparation methods for traditional SAMs and LDSAMs. The formation of LDSAMs involves an indirect strategy via the CT ester, which consists of a bulky spacer group.

7.15−7.40 (m); ^{13}C NMR (100 MHz, $CDCl_3$) δ 29.25, 29.40, 55.44, 113.23, 113.40, 127.99, 128.09, 129.08, 129.36, 129.64, 130.90, 132.35. [CT-MUA-DMT] ^{1}H NMR (300 MHz, $CDCl_3$) δ 1.17−1.29 (m), 1.62−1.69 (m), 1.79−1.88 (m) 2.12−2.17 (t), 2.31−2.37 (m), 2.66−2.71 (t) 3.34 (s), 3.74−3.80 (m), 3.90 (s), 3.95−3.99 (m) 6.69−6.85 (m) 6.94−6.99 (m) 7.08−7.60 (m) 7.74−7.86 (m); ^{13}C NMR (75 MHz, $CDCl_3$) δ 24.92, 25.83, 28.67, 29.18, 29.38, 29.55, 34.20, 39.52, 55.45, 55.74, 55.99, 68.19, 82.82, 113.25, 113.39, 113.80, 115.01, 116.24, 126.63, 127.61, 127.98, 128.23, 128.43, 129.34, 129.65, 129.99, 130.90, 131.58, 131.72, 132.16, 132.84, 137.77, 143.93, 145.75, 179.63. [CT-MUA] ^{1}H NMR (300 MHz, $CDCl_3$) δ 1.10−1.35 (m), 1.56−1.68 (m), 1.95−2.00 (t), 2.31−2.36 (t), 7.17−7.35 (m), 7.43−7.46 (m); ^{13}C NMR (75 MHz, $CDCl_3$) δ 24.92, 25.83, 28.67, 29.18, 29.38, 29.55, 34.20, 39.52, 52.68, 55.45, 55.74, 55.99, 68.19, 82.82, 113.25, 113.39, 113.80, 115.006, 116.243, 126.632, 127.611, 127.98, 128.23, 128.43, 129.34, 129.65, 129.99, 130.90, 131.58, 131.72, 132.16, 132.84, 137.77, 143.93, 145.75, 179.63. Electrospray mass spectrometry gave a mass-to-charge ratio of 517.1948 for the CT-MUA $[M + Na]^+$ adduct, consistent with a theoretical molar mass of 517.1944 g/mol calculated for the nondimerized product.

Substrate and SAM Preparation. Substrates were prepared using prime grade silicon wafers upon which were deposited a 4500 Å SiO_2 insulating layer, a 100 Å titanium adhesive layer, and a 1000 Å gold or silver outer layer. Photolithographic techniques were used to produce patterned devices with a defined 2.2 cm^2 surface area for monolayer assembly and a separate electrical contacting patch; these patterned devices were used for electrochemical impedance spectroscopy measurements, the results of which scale with surface area. Surface roughness of the substrates was <2 nm rms by atomic force microscopy. Substrates were rinsed with a sequence of absolute ethanol, deionized water, and absolute ethanol, then dried under a stream of N_2 prior to SAM preparation.

SAMs were prepared by immersion of the target region of the substrates in 1 mM ethanolic solutions of adsorbate for 48 h at room temperature. After incubation, samples were rinsed with a sequence of absolute ethanol, deionized water, and absolute ethanol, then dried under a stream of N_2.

LDSAMs were prepared by incubation of CT-MHA or CT-MUA monolayer samples in 50% trifluoroacetic acid in ethanol for 2 min, which results in cleavage of the acid-labile ester bonds between the chlorotrityl groups and the immobilized alkanethiolates. Following cleavage, the samples were rinsed with a sequence of absolute ethanol, deionized water, and absolute ethanol, then dried in a stream of N_2.

Instrumentation: EIS and FTIR Spectroscopy. EIS was performed using a standard three-electrode electrochemical cell (SAM sample as working electrode, saturated standard calomel electrode [SCE] as reference electrode, and platinum mesh as counter electrode) with N_2-purged PBS as electrolyte solution. A Gamry PCI4/300 potentiostat with EIS300 software module was used to take EIS measurements. The applied potential had an AC amplitude of 10 mV rms and a frequency range from 1 to 10^5 Hz, with DC bias potentials varying between 0 and +400 mV with respect to (wrt) SCE. The amplitude and phase angle of the current response were recorded at 10 points per decade in frequency.

Fourier transform infrared (FTIR) spectroscopy was performed using a liquid-nitrogen-cooled Thermo Nicolet 6700 spectrometer in 85° grazing angle mode with a 16 mm aperture. One hundred twenty eight scans were taken per sample at 4 cm^{-1} resolution.

Results and Discussion

Self-Assembly. In this study, LDSAMs of MHA and MUA prepared on gold and silver electrodes are compared to their traditional dense SAM analogues. Figure 1 outlines the direct self-assembly method for preparing regular SAMs of MHA and MUA, as well as the indirect assembly method for preparing LDSAMs. The indirect method was designed to circumvent the tendency of alkanethiolates to form tightly packed assemblies resembling two-dimensional crystals.[25,43,45] The approach involves a multistep process of conjugating MHA or MUA to bulky, space-filling CT groups to form CT-MHA or CT-MUA esters. The subsequent assembly of CT-MHA or CT-MUA monolayers on gold or silver is followed by cleavage of the

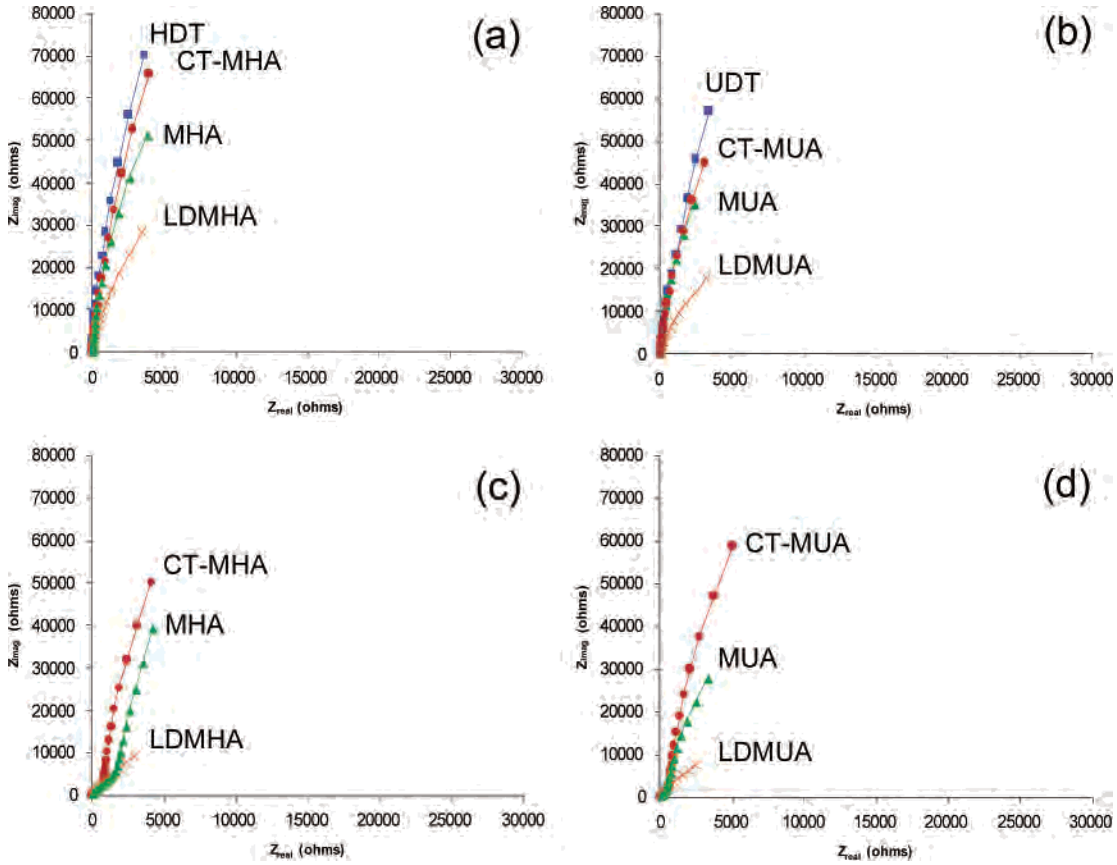

Figure 2. EIS Nyquist plots comparing different monolayer types. (a) C16 SAMs on Au, (b) C11 SAMs on Au, (c) C16 SAMs on Ag, and (d) C11 SAMs on Ag.

bulky CT groups, resulting in LDSAMs of MHA and MUA that are chemically identical to regular SAMs, but differ from the latter in the molecular spacing between the chains. Analysis of the CT-MHA and CT-MUA esters by NMR, mass spectrometry, and FTIR showed agreement of the thiols with the anticipated structures, verified the absence of disulfide dimers, and demonstrated the esters' stability for several months, when stored under inert gas at −20° C.

Electrochemical Impedance Spectroscopy. Figure 2 shows EIS Nyquist plots acquired in PBS buffer (pH 7.4) at 0 mV DC (wrt SCE) for various types of monolayers on gold and silver. When we compare different types of monolayers with the same chain length and on the same substrate, we notice that the highest impedances are seen with the dense CH_3-terminated SAMs (HDT and UDT) followed by the CT-terminated SAMs (CT-MHA and CT-MUA), then the dense COOH-terminated SAMs (MHA and MUA), and finally the LDSAMs (LDMHA and LDMUA). As expected, hydrophobic headgroups and higher packing densities result in greater ionic barrier properties. The greater impedance of the CT-terminated SAMs compared to MHA/MUA can be attributed to the dense packing of the large, hydrophobic CT groups on the surface. Although the impedance of the LDSAMs is low relative to the other monolayers, it is significantly higher than that of bare gold or silver; the impedance modulus at 1 Hz (maximum *y*-axis value) of bare gold and silver is on the order of 1000−2000 Ω (too low to be clearly plotted in Figure 2), which is significantly lower than the most permeable LDSAM of LDMUA on Ag, which has a modulus of 7500 Ω at 1 Hz. This observation suggests the relative homogeneity and continuity of the LDSAMs, with a lack of gross levels of pinhole defects. When we compare the impedance of monolayers with different chain lengths (Figure 2a vs 2b), we typically see higher impedances for the C16-length SAMs than for the corresponding C11-length monolayers. This observation is expected because of the greater resistance to ionic permeation that monolayers with longer chain lengths display.[39] Similarly, monolayers assembled on gold typically showed higher impedances than monolayers assembled on silver (Figure 2a vs 2c). Also noticeable in the Nyquist plots of SAMs on silver are some deviations from linearity in the slope of the data; greater phase angle deviations are seen for the data taken at lower frequencies (closer to the origin). Since solution resistance is the dominant source of impedance at low frequencies, this effect could result from oxidation at the surface of the silver due to trace levels of dissolved oxygen in the PBS solution.

Impedance Switching. The next series of EIS analyses examined the effect of the applied DC potential on monolayer impedances. During these experiments, a series of increasingly positive DC electrical potentials was applied during EIS measurements. Because our LDSAMs have enhanced conformational freedom,[23] we would anticipate the application of positive potential to more easily influence the structure of the monolayers and thus alter their impedance profiles to a greater degree compared to the more sterically hindered dense SAMs.

Nyquist plots of the potential responses of SAMs on gold are shown in Figure 3. The measurements for each type of monolayer were performed consecutively, in order of increasing positive potential, without removing the sample from the electrochemical cell during the experiments. An electrochemical potential of +400 mV wrt SCE was chosen as the upper potential limit to avoid electrochemical oxidation of the thiol or potential-induced monolayer defects.[40] In the case of both (a) the C16- and (b) the C11-length monolayers, the impedance of dense SAMs does not change significantly upon application of potentials up to +400

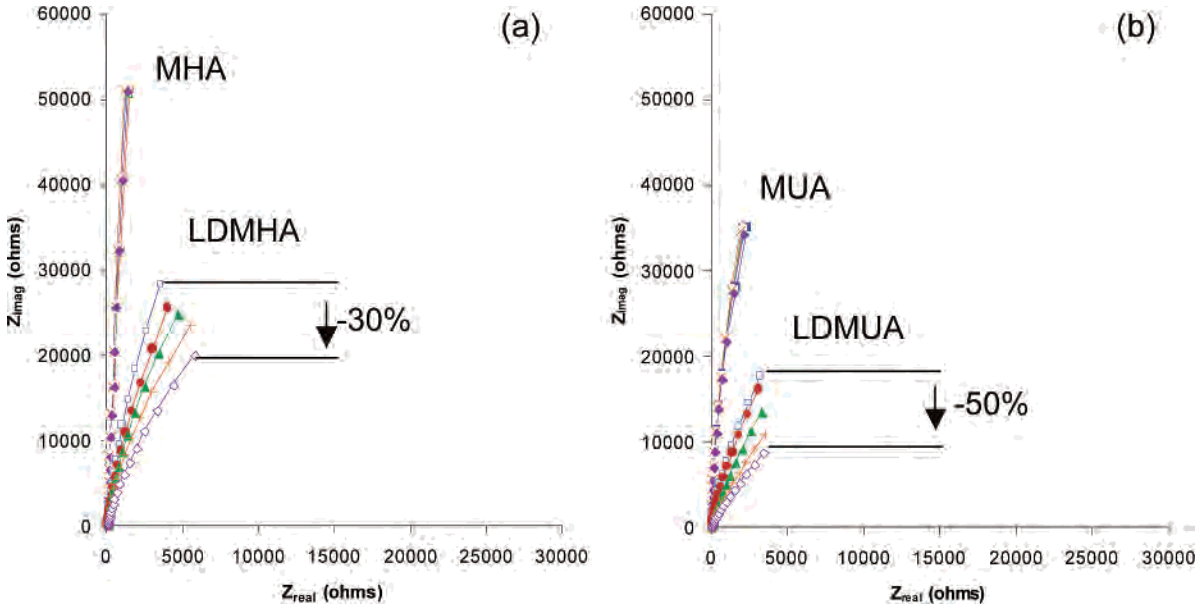

Figure 3. Impedance response of monolayers on Au to a stepwise change in electrical potential between 0 and +400 mV wrt SCE. (a) C16 monolayers and (b) C11 monolayers.

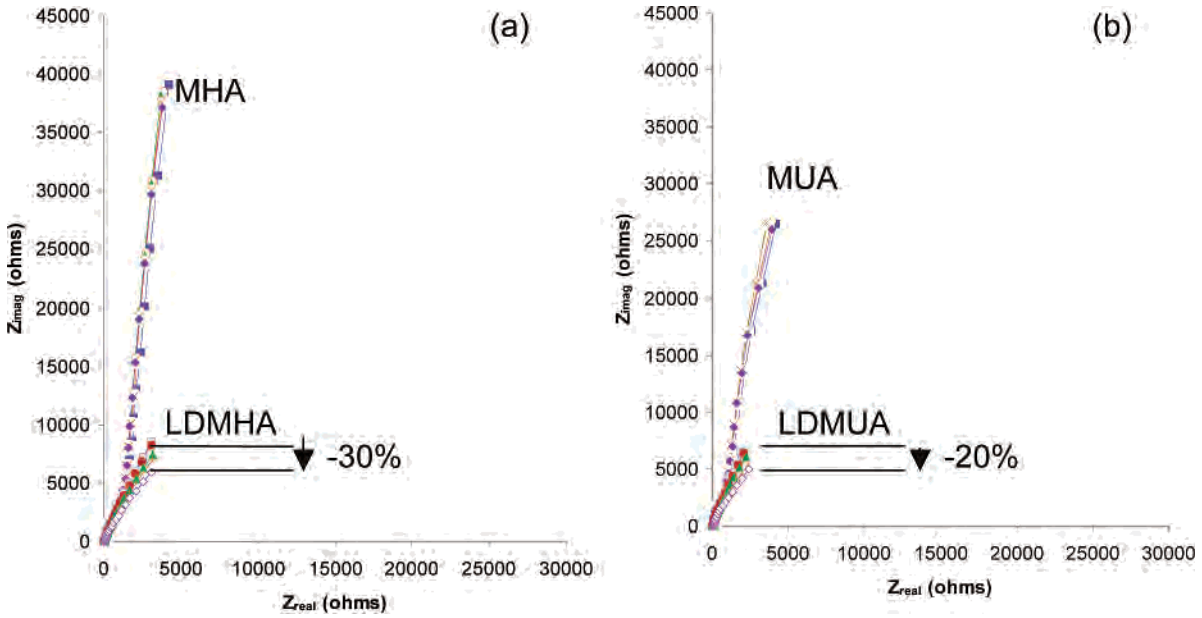

Figure 4. Impedance response of monolayers on Ag to a stepwise change in electrical potential between 0 and +40 mV wrt SCE. (a) C16 monolayers and (b) C11 monolayers.

mV, while the impedance of the LDSAMs decreases stepwise with increasing positive potential, culminating in a decrease in impedance modulus (*y*-axis value) of about 30% for LDMHA at +400 mV and about 50% for LDMUA at +100 mV. LDSAMs of MUA thus showed greater sensitivity to the application of the electrochemical potential than LDSAMs of MHA. These data are in agreement with an increased flexibility of the shorter-chain LDSAMs. The increase of phase angle (trace tilt) seen for LDSAMs at higher potentials also indicates increasingly greater deviations from ideal capacitor behavior and increasing ionic permeability as a result of the conformational transitions induced by the applied potential.

The potential responses of SAMs on silver are shown in Figure 4. In this case, +40 mV wrt SCE was chosen as an upper potential limit because of the increased potential sensitivity of the SAMs on silver (gross deformation of the impedance traces are seen at +60 mV, data not shown). Although the potential response trends were similar to those of SAMs on gold, some differences are apparent. The dense SAMs appear to be somewhat more sensitive to potential than the corresponding monolayers on gold. The effect of applied potential on LDMUA is also relatively small, possibly because of the shorter chain length of this monolayer. The very high level of conformational flexibility that results from this structure may obscure the effect of actively induced conformational transitions.

The results from Figures 3 and 4 generally suggest that the impedance of LDSAMs, unlike that of dense SAMs, can be controlled or tuned across a relatively wide range through the application of small electrical potentials.

After demonstrating the tunability of LDSAMs, we conducted a series of EIS experiments to test the reversibility of the electrical impedance response of LDSAMs—a property which could be useful for technological applications. Previous studies have demonstrated the reversible switching of LDSAMs on gold,

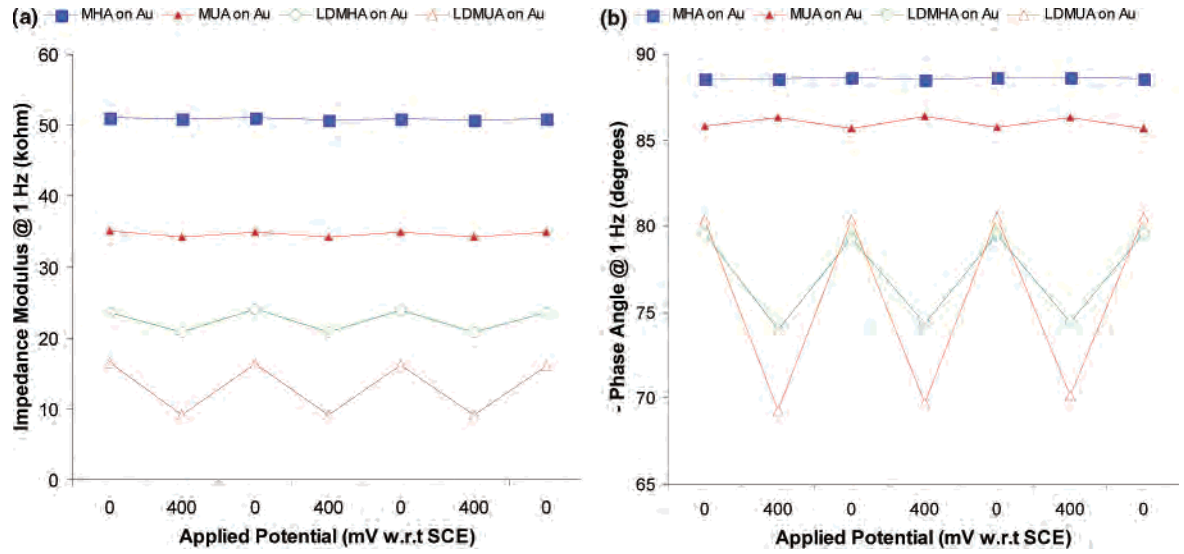

Figure 5. Reversibility of the impedance response for potential switching between 0 and +400 mV wrt SCE for monolayers on Au. (a) Impedance modulus vs frequency and (b) phase angle vs frequency.

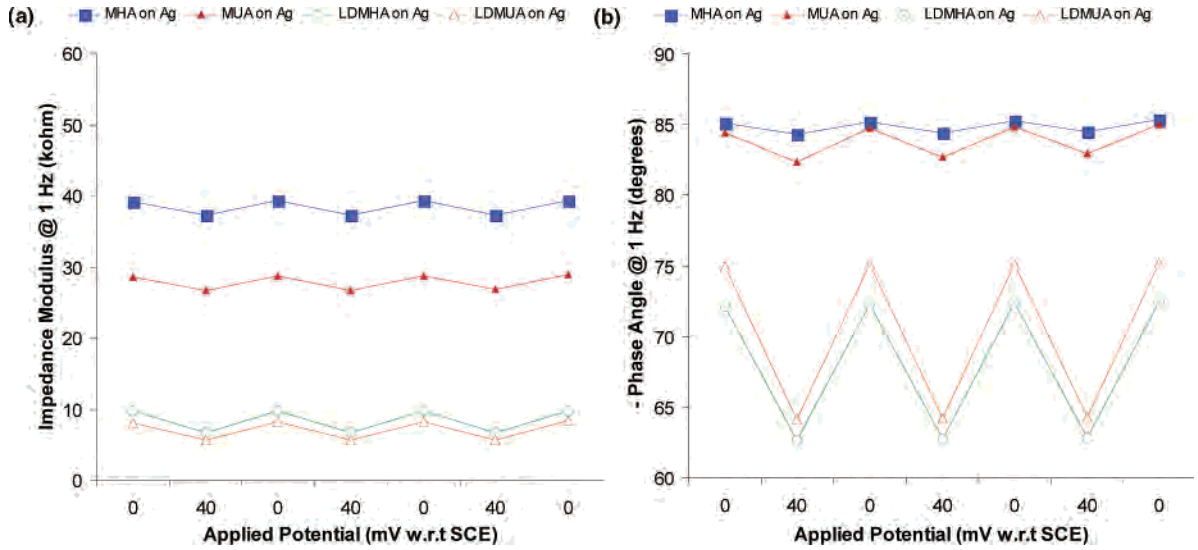

Figure 6. Reversibility of the impedance response for potential switching between 0 and +40 mV wrt SCE for monolayers on Au. (a) Impedance modulus vs frequency and (b) phase angle vs frequency.

conferring dynamic control over surface properties such as wettability.[23] The present experiments address reversible switching of the DC bias potential during EIS analysis between 0 and +400 mV wrt SCE for all Au monolayers (except LDMUA, for which it was between 0 and +100 mV). In contrast, the DC bias potential was switched between 0 and +40 mV wrt SCE for all Ag monolayers. The concurrent EIS analysis provides an assessment of reversible control over ionic conduction through the monolayer.

Figure 5 shows the resulting pattern of impedance moduli and phase angles at 1 Hz from the series of experiments on Au SAMs. Toggling the potential through four switching cycles has the least effect on dense MHA SAMs, whereas MUA SAMs show only a slight response. LDMHAs show a pronounced response, and LDMUAs exhibit the strongest response. The effect is generally similar for impedance modulus and phase angle, although interestingly, with MUA we see a slight inversion effect where the phase angle is marginally higher at +400 mV. The greater responsiveness of the C11 SAMs and the LDSAMs is consistent with our previous observations of the effect of monolayer chain length and density on impedance. Reversibility is very good, with little drift seen in impedance levels over the course of the measurement sequence.

Figure 6 shows the resulting pattern of impedance moduli and phase angles at 1 Hz from the series of experiments on Ag SAMs. Here we see increased potential sensitivity to smaller applied fields but also less dramatic contrast between dense SAMs and LDSAMs. The data show excellent reversibility, again with very little drift of the impedance levels over the course of the experiment.

The data shown in Figures 5 and 6 suggest that conformational flexibility is essential to producing monolayer systems with reversible impedance properties. Although the flexibility conferred by the Ag lattice is clearly sufficient to yield reversibility trends, more distinctly contrasting effects are seen on Au, when comparing LDSAMs with dense SAMs.

Fourier Transform Infrared Spectroscopy. Grazing angle FTIR spectra were recorded for dense SAMs and LDSAMs before and after the EIS reversibility cycling experiments in order to assess the effect of EIS on monolayer integrity and stability. Spectra for Au monolayers are shown in Figure 7, spectra for Ag monolayers are shown in Figure 8, and characteristic

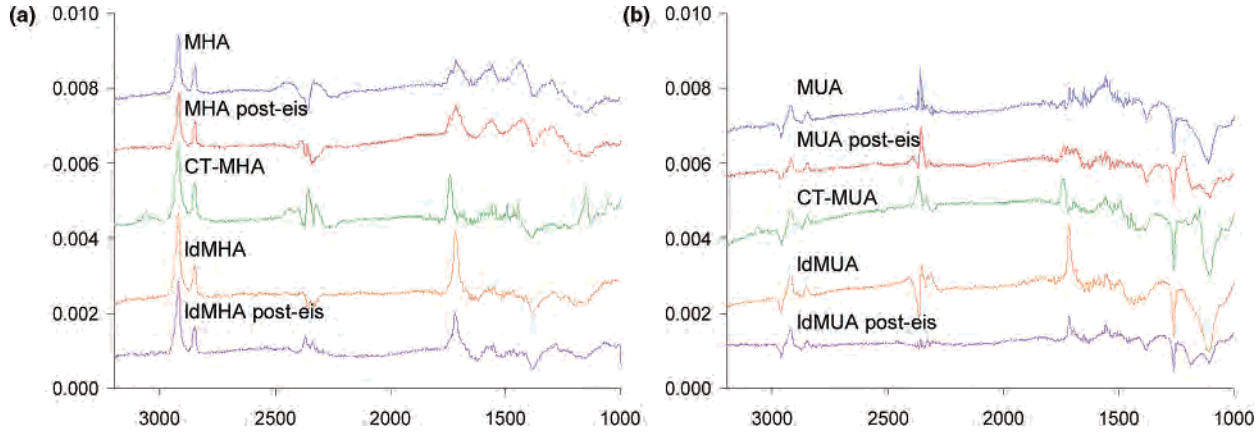

Figure 7. FTIR spectra of several monolayers on Au. (a) C16 monolayers and (b) C11 monolayers.

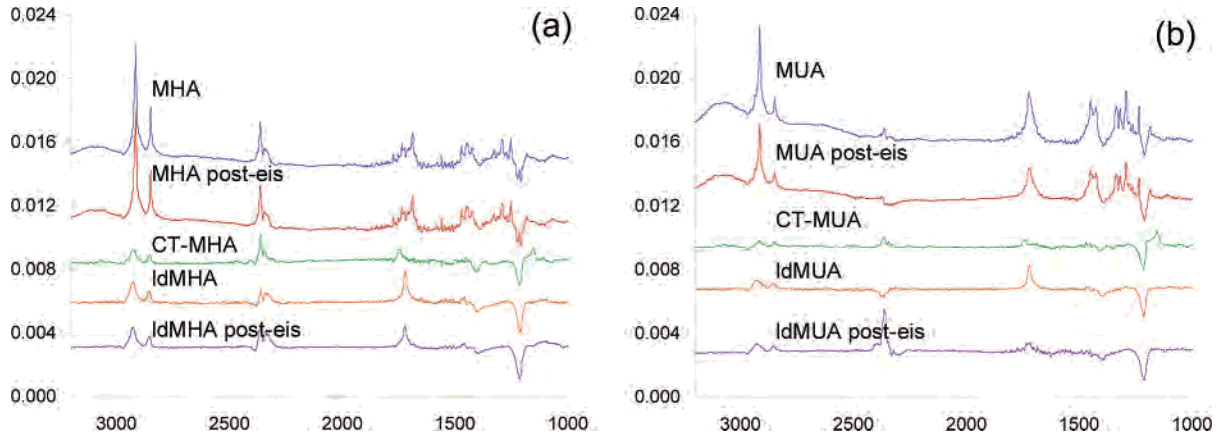

Figure 8. FTIR spectra of several monolayers on Ag. (a) C16 monolayers and (b) C11 monolayers.

Table 1. FTIR Peak Locations for Several Monolayers Assembled on Au and Ag

monolayer	substrate	asym C−H	sym C−H	asym CH_2	sym CH_2	C═O, carbonyl	C−O, ester	C−Cl
MHA	Au	–	–	2919.6	2850.9	1716.2	–	–
MHA-post-EIS	Au	–	–	2919.0	2850.5	1717.7	–	–
CT-NHA	Au	3063.2	3032.6	2921.9	2851.6	–	1743.5	1153.1
LDMHA	Au	–	–	2921.3	2852.0	1720.0	–	–
LDMHA post-EIS	Au	–	–	2920.8	2851.5	1720.1	–	–
MUA	Au	–	–	2922.4	2841.0	1717.5	–	–
MUA-post-EIS	Au	–	–	2921.8	2850.2	1718.1	–	–
CT-MUA	Au	3066.37	3028.8	2922.9	2853.2	–	1743.0	1154.6
LDMUA	Au	–	–	2925.3	2855.3	1718.6	–	–
LDMUA post-EIS	Au	–	–	2923.1	2852.1	1717.8	–	–
MHA	Ag	–	–	2913.9	2846.6	1687.8	–	–
MHA-post-EIS	Ag	–	–	2914.3	2847.2	1686.2	–	–
CT-NHA	Ag			2923.2	2851.0		1741.8	1154.2
LDMHA	Ag	–	–	2925.1	2853.4	1718.4	–	–
LDMHA post-EIS	Ag	–	–	2926.7	2853.7	1720.2	–	–
MUA	Ag	–	–	2913.4	2846.3	1720.7	–	–
MUA-post-EIS	Ag	–	–	2913.3	2846.2	1720.6	–	–
CT-MUA	Ag			2915.0	2847.9	–	1745.7	1153.0
LDMUA	Ag	–	–	2923.9	2854.8	1718.6	–	–
LDMUA post-EIS	Ag	–	–	2928.9	2853.5	1720.8	–	–

peak locations are listed in Table 1. Dense monolayers have characteristic asymmetric and symmetric methylene CH_2 stretches at ∼2920 and ∼2850 cm^{-1}, as well as C═O stretches at ∼1720 cm^{-1}. Chlorotrityl-terminated monolayers show additional peaks at ∼3060 and ∼3030 cm^{-1} (asymmetric and symmetric aromatic C−H stretch) and ∼1150 cm^{-1} (C−Cl stretch), as well as a shift of the C═O stretch from 1720 to ∼1740 cm^{-1} due to the ester bond. Details of the FTIR studies are given in Table 1. After CT group cleavage, LDSAMs show an absence of the previously present aromatic and C−Cl stretches, a C═O shift to the ∼1720 cm^{-1} carbonyl range, and generally minimal shifts in CH_2 stretches, with the exception of LDSAMs of MUA on Ag. LDSAMs show a red-shift in their CH_2 stretches compared to dense MHA and MUA monolayers. This shift reflects the more fluid and less crystalline environment experienced by the methylene groups within low-density monolayers and is also the reason Ag monolayers show a greater red-shift than Au monolayers.

With the exception of a slight shift in the asymmetric CH_2 stretch for LDSAMs of MUA on Ag, there is no difference

between the spectra recorded before and after impedance switching. The data generally suggest that the repeated application of small electrical potentials does not affect the integrity of LDSAMs.

Conclusions

Low-density monolayers of MHA can be prepared via self-assembly of bulky precursor thiols and subsequent cleavage of the spacer.[23] Compared to their dense counterparts, these monolayers show enhanced responsiveness to the application of even small electrical potentials.[23] Although previous studies have focused on LDSAMs assembled on gold,[23] we have now extended this concept to shorter thiols (MUA) self-assembled on gold and to LDSAMs of MHA and MUA on silver substrates. Moreover, we have demonstrated that the application of small electrical potentials can induce switching of the electrochemical barrier properties of these monolayers. EIS conducted in PBS buffer at physiological pH values has proven to be an exquisite method for studying reversible transitions in low-density monolayers. Moreover, the switching of the four LDSAMs (MHA and MUA on Au and Ag) was found to be in clear contrast to the regular SAMs of MHA and MUA that were included in this study as references. In fact, the stepwise application of electrochemical potentials between 0 and +400 mV wrt SCE for Au and between 0 and +40 mV wrt SCE for Ag enabled a fine-tuning of the impedance of LDSAMs. The potential-induced changes in impedance were found to be reversible, as demonstrated by the repeated switching of LDSAMs of MHA and MUA on both gold and silver electrodes. The stability of the LDSAMs during the impedance switching was verified by comparing the grazing angle FTIR spectra of the LDSAMs before and after impedance switching. Within the margins of error, these spectra were identical. LDSAMs show an interesting responsiveness to the application of small electrical potentials. The herein-demonstrated ability to tune and switch their impedance properties may be useful, when considering their potential for biosensors or active biointerfaces for cell-based studies. Much future work is needed before these applications become reality, however.

Acknowledgment. We thank Hsien-Yeh Chen, Onnop Srivannavit, Brian Johnson, and Kenneth Chomistek for help with electrode microfabrication. D.K.P. acknowledges support from a graduate fellowship from the National Institutes of Health through the University of Michigan Cellular Biotechnology Training Program. The project was funded by grants from the National Institutes of Health and an Idea Award of the Department of Defense.

LA061677O